Ocean Wave Integral Parameter Measurements Using Envisat ASAR Wave Mode Data

Xiao-Ming Li, Susanne Lehner, and Thomas Bruns

***Abstract*—An empirical algorithm to retrieve integral ocean wave parameters such as significant wave height (SWH), mean wave period, and wave height of waves with period larger than 12 s (H_{12}) from synthetic aperture radar (SAR) images over sea surface is presented. The algorithm is an extension to the Envisat Advanced SAR (ASAR) wave mode data based on the CWAVE approach developed for ERS-2 SAR wave mode data and is thus called CWAVE_ENV (CWAVE for Envisat). Calibrated ASAR images are used as the only source of input without needing prior information from an ocean wave model (WAM) as the standard algorithms used in weather centers. This algorithm makes SAR an independent instrument measuring integrated wave parameters like SWH and mean wave period to altimeter quality. A global data set of 25 000 pairs of ASAR wave mode images and collocated reanalysis WAM results from the European Centre for Medium-Range Weather Forecasts (ECMWF) is used to tune CWAVE_ENV model coefficients. Validation conducted by comparing the retrieved SWH to *in situ* buoy measurements shows a scatter index of 0.24 and 0.16 when compared to the ECMWF reanalysis WAM. Two case studies are presented to evaluate the performance of the CWAVE_ENV algorithm for high sea state. A North Atlantic storm during which SWH is above 18 m as observed by SAR and Radar Altimeter simultaneously is analyzed. For an extreme swell case that occurred in the Indian Ocean, the potential of using SWH measurements from ASAR wave mode data derived by the CWAVE_ENV algorithm is demonstrated.**

***Index Terms*—Empirical algorithm, integral wave parameter, synthetic aperture radar (SAR), wave mode data.**

I. Introduction

OCEAN waves are the ocean's most obvious surface feature, which interact with atmosphere, ocean currents, bottom topography, and with one another. For many reasons, an understanding of their statistical properties is required, such as marine transportation, global sea state statistics, and its changes, as well as ocean wave parameters in specific locations for harbor and ocean engineering, ship design, and coastal protection.

Ocean waves are traditionally measured *in situ* at one point, as by moored buoys, which are normally located near to coast, giving very limited spatial coverage. Satellite remote sensing, particularly active microwave sensors, e.g., synthetic aperture radar (SAR) and radar altimeter (RA), offers alternate approaches to observe ocean surface waves on a global scale. SAR is a unique sensor that can provide 2-D ocean surface information with high spatial resolution, independent of cloud cover and daytime.

The L-band SAR sensor onboard SEASAT launched in 1978 provided a first realization of global ocean surface measurements from space (see [1]). From 1991 until now, the ERS-1, ERS-2, and Envisat missions launched by the European Space Agency (ESA) have operationally provided continuous SAR ocean wave measurements. On these platforms, SAR and RA are onboard jointly. In principle, two completely independent surface wave measurements from space are available. While the altimeter measurements are acquired at nadir, the SAR measurements are taken at about 300 km away looking to the right. Therefore, these double tracks provide simultaneous sea state measurements, which is particularly useful for extreme sea state validation in storms with strong gradient in wave height field. Both measurements can be used jointly for wave climate analysis, reducing the limitation of spatial sampling. Aside from the assimilation of RA measurements at nadir track, SAR can provide another source of observation as an additional quality control for data assimilation in numerical wave models (WAMs).

The measurement of significant wave height (SWH) by altimeters is well established, and the retrieved accuracy is comparable to that of *in situ* buoy measurements, e.g., [2] and [3]. In addition to SWH, mean wave period is another important sea state parameter. Unlike the approach for SWH measurements, retrieval of wave period from RA is still under development. Several empirical models, e.g., [4]–[6], have been proposed to obtain wave period measurements from altimeter data.

Following an overview of sea state measurements from RA data, the current algorithms to derive the 2-D ocean wave spectra from SAR are briefly summarized. A new method to derive integral wave parameters from Advanced SAR (ASAR) images is presented.

A. Ocean Wave Measurements From SAR

Nonlinear Retrieval Approach: The mechanisms of SAR imaging sea surface gravity waves generally consist of the linear approaches of tilt and hydrodynamic modulation, as well as the nonlinear distortion induced by the radial wave motions [7]. This leads, among other effects, to image smearing and to a loss of information beyond the so-called azimuth cutoff wavelength [8]. For ERS and Envisat SAR, this corresponds typically to wavelengths shorter than about 200 m in the along-track

Manuscript received December 21, 2009; revised April 23, 2010; accepted May 23, 2010. Date of publication July 12, 2010; date of current version December 27, 2010.

X.-M. Li and S. Lehner are with the Remote Sensing Technology Institute, German Aerospace Center (DLR), 82234 Wessling, Germany (e-mail: Xiao.Li@dlr.de; Susanne.Lehner@dlr.de).

T. Bruns is with Seeschifffahrtsberatung, German Weather Service (DWD), 20359 Hamburg, Germany (e-mail: Thomas.Bruns@dwd.de).

Color versions of one or more of the figures in this paper are available online at http://ieeexplore.ieee.org.

Digital Object Identifier 10.1109/TGRS.2010.2052364

direction. In addition, ocean wave spectra from satellite SAR images suffer from a basic 180° ambiguity of wave propagation direction, which can be resolved by using complex data [9]. A nonlinear mapping of ocean wave spectra into SAR image spectra, as well as its inversion, was developed by Hasselmann and Hasselmann [10] and is referred to as the Max Planck Institute (MPI) scheme in the following. This inversion algorithm accomplishes the retrieval of ocean wave spectra from SAR spectra within the computational constraints of real-time operational applications (see also [11] for a simpler transform). An assessment of the performance of the algorithm, as well as the operational feasibility, was given by Heimbach *et al.* [12] using three-year (1993–1995) ERS-1 SAR wave mode User WAve spectrum (UWA) spectral data (i.e., SAR image spectrum in polar grid; see [13]). Validation results show that approximately 75% of SAR UWA spectral data were converted into successful retrievals. There remains a small overestimation of less than 0.5 m for retrieved SWH by the MPI scheme compared to the results from a WAM.

A semiparametric algorithm was developed as well for retrieving complete ocean wave spectra from SAR by taking into account the ERS SAR wave mode image spectra and collocated wind vectors from ERS wind scatterometer as additional input [14]. The algorithm could not be used for the Envisat mission on which the scatterometer is not onboard.

A parametric inversion scheme for the derivation of 2-D ocean wave spectra from SAR look cross spectra is presented by Schulz-Stellenfleth *et al.* [15] and is referred to as the Partition Rescaling and Shift Algorithm (PARSA) algorithm. This algorithm needs prior information from a numerical WAM as well, while using the complex information of SAR data to resolve the ambiguity on wave propagation direction.

SAR Cross-Spectral Algorithm: Taking two looks of SAR wave mode complex data, the cross spectra can be derived to remove the 180° ambiguity of ocean wave propagation direction [9], which is demonstrated on airborne C-band SAR data. Furthermore, the speckle noise is reduced significantly, e.g., as described by Lehner *et al.* [16].

This method has been adopted by ESA for the ASAR wave mode data, the so-called WVW Level 2 products [17]. Ocean wave spectra of the WVW products only yield information in the inner spectral bins contained in the ASAR wave mode data, and inverted SWH has a significant bias of −0.22 m and a scatter index (SI) of 33% as compared to *in situ* buoy measurements [18].

To some extent, the PARSA algorithm mentioned earlier is the combination of the nonlinear approach and the cross-spectral algorithm. It uses the cross spectrum of two SAR looks to remove the 180° ambiguity and blends the SAR image spectra and first prior information from a WAM.

Empirical Algorithm: For the current nonlinear or quasi-linear algorithms retrieving 2-D ocean wave spectra from SAR imagery, either prior information from a numerical WAM is needed, e.g., the MPI or PARSA scheme as used at weather forecast centers where a first guess is available or when no first guess information is taken like the ESA WVW products; the provided information on wave height is limited to part of the spectrum for waves longer than a certain threshold.

A new empirical algorithm called CWAVE_ERS [17] to derive ocean wave integral parameters, instead of the full 2-D spectra, without needing prior information was proposed for the reprocessed ERS-2 SAR wave mode data [16]. Validation results show that the performance of CWAVE_ERS is fairly good when compared to the European Centre for Medium-Range Weather Forecasts (ECMWF) WAM using 6000 collocation data pairs and to 21 buoy measurements during three weeks in 1996. For both comparisons with respect to SWH, results of CWAVE_ERS showed that the root mean square (rms) is 0.44 and 0.39 m, respectively. The performance of CWAVE_ERS for high sea state, e.g., SWH higher than 6 m, is not evaluated in the comparisons.

B. New Empirical Algorithm CWAVE_ENV

For more than 17 years, SAR global ocean observation data have been acquired since the launch of ERS-1 in 1991. Using the CWAVE approach, another independent active satellite measurement of sea state parameters thus becomes available, contributing global wave climate analysis in addition to the RA data.

In this study, an extended empirical algorithm called CWAVE_ENV (CWAVE for Envisat) to derive integral wave parameters from Envisat ASAR wave mode data is presented. The CWAVE_ENV empirical geophysical model function is adopted from CWAVE_ERS for ERS-2 reprocessed SAR wave mode data. Considering that ASAR has a different spatial resolution, image size, calibration constant, and capabilities for imaging ocean surface to ERS-2 SAR, newly tuned coefficients for the CWAVE_ENV model are needed.

Previous research states that, due to the cutoff effect of the SAR imaging mechanism, only long-wave information is imaged by SAR, which is apparent for high-altitude orbit SAR systems like ERS SAR and Envisat ASAR. Still here, we show that the wave parameters corresponding to the complete spectrum like SWH can be retrieved well not only in low to moderate sea state but also in high sea state from the ASAR image by using the empirical model without needing prior information.

This paper is organized as follows. In Section II, the data set used in this study is introduced. Section III contains the empirical model tuning and validation. Global sea state statistics derived from the ASAR wave mode data acquired in December 2006 and January and February 2007 are compiled in Section IV. Two case studies, a North Atlantic storm generating wind seas with SWH above 18 m and a high ocean swell case with maximum wave height above 11 m in the Indian Ocean, are presented in Section V. Finally, summary and conclusions are given.

II. Description of Data Sources

A. Envisat ASAR Wave Mode Data

When ASAR is operated in the wave mode, small images covering 6 km × 5 km to 10 km × 5 km are acquired along the orbit every 100 km.

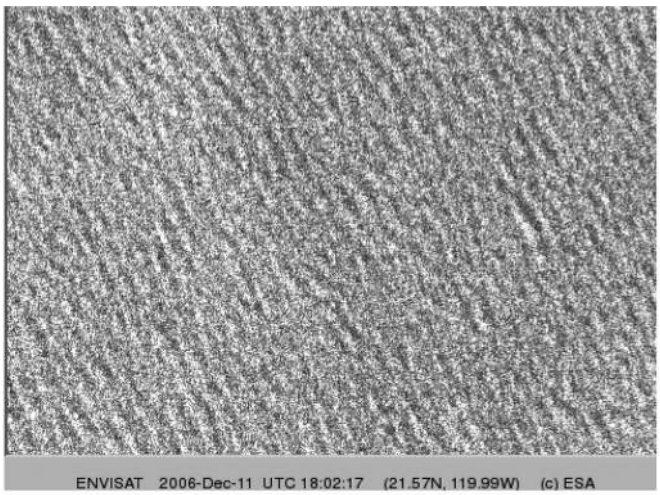

Fig. 1. Examples of Envisat ASAR wave mode data acquired over sea surface for (a) the homogenous case and (b) the inhomogeneous one.

In the present study, the following filters are applied on the ASAR wave mode data chosen for the tuning and validation of the CWAVE_ENV model.

1) The ASAR wave mode data are generally acquired in the IS2 swath with incidence angles at around 23° and VV polarization. During the experimental period of January 24 to February 6, 2007, ASAR was requested to obtain wave mode data in the IS4 swath, i.e., with an incidence angle of around 33°. These data are excluded from the data set used in the present study.
2) To avoid effects of sea ice in the north and south polar regions, the wave mode data acquired between $-70°$ S and 70° N are included.
3) A homogeneity test is performed on the ASAR wave mode data. Examples of homogenous ASAR wave mode data and inhomogeneous one are shown in Fig. 1(a) and (b), respectively.

The ratio of image variance and squared image mean is set to 1.05 as a threshold to classify the ASAR wave mode images into homogenous or inhomogeneous cases [20]. Around 9% ASAR imagettes acquired in December 2006 fail to pass the homogeneity test due to surface features, and they are excluded from the tuning data set.

B. Numerical WAM Data

A summary of the third-generation WAM is given in the report of the WAMDI Group [21]. From June 1992, a new version of WAM (called cycle 4 [22]) was introduced operationally at ECMWF. For global ocean forecast, the horizontal resolution of WAM operated in ECMWF can reach 1.5°, and for regional forecast, a higher resolution model up to 10 km can be provided, e.g., the WAM version operated in the German Weather Service (DWD).

The basic equation that is used in the WAM is the action balance equation

$$\frac{\partial N}{\partial t} + \vec{c}_g \frac{\partial N}{\partial \vec{\mathbf{x}}} = \sum_i S_i \tag{1}$$

in which $N(\vec{\mathbf{x}}, t, f, \theta)$ is the wave action and is equal to $E(\vec{\mathbf{x}}, t, f, \theta)/\omega$, where E is the directional wave spectrum in frequency f and direction θ and ω is the radial frequency. $\vec{c}_g$ is the group velocity of the wave component. S_i is the net source function, consisting of three terms: $S_{\rm in}$ is the energy input by wind, $S_{\rm nl}$ is the nonlinear energy transfer by wave–wave interactions, and $S_{\rm ds}$ is the high-frequency dissipation.

Integral wave parameters SWH and mean wave period (zero upcrossing period used in this study) can be derived from 2-D wave spectra of the model as given in

$$H_s = 4\sqrt{\int E(f,\theta) df d\theta} \tag{2}$$

$$T_{m02} = \sqrt{\int E(f,\theta) df d\theta \Big/ \int E(f,\theta) f^2 df d\theta}. \tag{3}$$

Performance of operational WAM forecast has been improved considerably. During 1992–1993, the rms error (rmse) of the 24-h forecast of ECMWF was around 0.75 m for SWH, which has been reduced to 0.25 m in 2002–2003, due to the assimilation of sea state and surface wind observations provided by satellite sensors, e.g., RA, SAR, and Scatterometer [23]. The accuracy of some regional numerical WAMs is validated as well in extreme sea state, for instance, the Local Sea wave Model operated by DWD. This was tested, e.g., in selected severe winter storms over the North and the Baltic Sea, giving reasonable quality for short-period forecasts [24].

However, with respect to the long-term accuracy of global WAMs, there is still room for improvement, as shown in the validation for the reanalysis ERA-40 wave products. SWH is slightly overestimated for low sea state ($<$ 1.5 m) and substantially underestimated by more than 20% for rough sea state, when compared to the RA onboard TOPEX/Poseidon and *in situ* buoy measurements [25].

In the present study, the provided operational ECMWF wave spectra output on a 1.5° by 1.5° longitude–latitude grid at 6-h synoptic times. The WAM spectra are provided on a polar grid with 24 directional bins and 30 frequency bins beginning from 0.03452 Hz with a logarithmic increment of 1.1 Hz. It needs

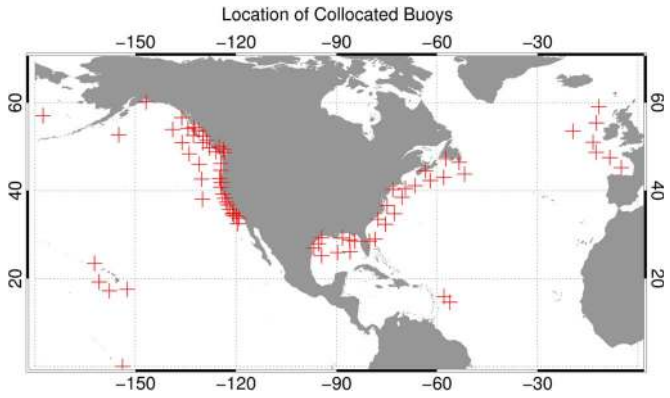

Fig. 2. Location of collocated buoys used for CWAVE_ENV model validation.

to be pointed out that satellite observation of wind and wave has been assimilated in the ECMWF WAM. It is referred to as the ECMWF reanalysis model in the following. Sea state parameters integrated from the 2-D WAM wave spectra are collocated to individual ASAR data points using a ±3-h time window and a 200-km distance window.

DWD provides integral wave parameters on grid points instead of full 2-D spectra. The spatial and temporal resolutions of the model are 0.75° and 3 h, respectively. Validation of SWH derived from the DWD 24-h-forecast Global Sea wave Model (GSM) WAM shows good agreement with a positive bias of 0.04 m and an SI of 0.20 when compared to buoy measurements during June–August 2007 [26].

C. Buoy Data

Fig. 2 shows a map of the 77 buoys used as the *in situ* validation data set. Most of the buoys are maintained by the National Oceanic and Atmospheric Administration National Data Buoy Center (NDBC) and the Environment Canada Marine Environmental Data Service.

The nondirectional buoys are used to measure sea surface vertical acceleration, which can be used to derive surface displacement spectra. The details of the data collection and analysis procedures for the NDBC nondirectional wave buoys are described in [27]. Generally, in each hour, a 20-min record of vertical hull accelerations of the buoy, sampled at a rate of 1 Hz, is collected. By applying a segmented fast Fourier transform (FFT) for the record, an acceleration spectrum is calculated from which the nondirectional wave spectrum $S(f)$, i.e., frequency spectrum, is obtained.

Integral wave parameter, e.g., SWH, can be estimated from the frequency spectrum $S(f)$ using an interval $[f_0, f_1]$ of frequencies

$$SWH = 4\left[\int_{f_0}^{f_1} S(f)df\right]^{1/2}. \tag{4}$$

For practice, numerically, the frequencies range from 0.03 to 0.40 Hz at intervals of 0.01 Hz.

Name, latitude, and longitude information of the buoy stations, as shown in Fig. 2, are given in Appendix A.

D. Summary of the Data Set Used in Tuning and Validation

Several data sets are used in the present study for algorithm tuning and validation, as well as for case studies.

ASAR wave mode data

—Data acquired during the full month of December 2006 are used as the tuning data set of the CWAVE_ENV algorithm, excluding 347 wave mode data collocated to *in situ* buoy measurements. They are also used as the data set to evaluate the goodness of fit of the CWAVE_ENV model.

—Data acquired during January, February, and May 2007 are used separately for validation of the algorithm.

Numerical WAM data

—Results of the ECMWF reanalysis WAM are used for tuning and validation of the CWAVE_ENV algorithm.

—Results of the DWD forecast WAM are used for comparisons. No wave observations are assimilated in the WAM itself before March 2008.

In situ measurements

—They are acquired from the meteorological buoys, so they are independent measurements.

Crossover RA measurements

—They are derived from the RAs of GEOSAT Follow-On (GFO) and JASON used as an independent validation source.

III. CWAVE_ENV Model Tuning Approach

In this section, the CWAVE_ENV parametric model structure, model fitting procedure, and its evaluation using the tuning data set are described in detail.

A. Introduction of the Parametric Model

The CWAVE_ENV model is built based on the multiple-regression method.

Multiple-Regression Model: ASAR image parameters collected in vector $\mathbf{S}(s_1, \ldots, s_{ns})$ are supposed to be related to sea state measurement W with coefficient vector $\mathbf{A}(a_0, a_1, \ldots, a_{ns})$. A simple linear regression model collecting these parameters to be used as an estimator is expressed by (see [28])

$$W = a_0 + \sum_{i=1}^{n_s} a_i s_i + E_i \tag{5}$$

where E_i are random variables with zero mean.

In order to also include nonlinearities, as well as possible coupling, among different ASAR image parameters, a quadratic term is added on the right-hand side of (5) as shown in

$$W = a_0 + \sum_{1\le i\le n_s} a_i s_i + \sum_{1\le i\le j\le n_s} a_{i,j} s_i s_j \tag{6}$$

which is the geophysical model function used in the CWAVE_ENV algorithm.

The model states that the sea state parameter W is expressed as linear combinations of ASAR image parameters

$\mathbf{S}(s_1, \ldots, s_{ns})$ with the extended coefficient vector $\mathbf{A}(a_0, \ldots, a_{ns}, a_{11}, \ldots, a_{n_s a_{n_s}})$ in a dimension of $n_A = 0.5(n_s^2 + 3n_s + 2)$. However, the parameters themselves can be nonlinear functions of other variables. In the following, the ASAR parameters chosen in the CWAVE_ENV model are introduced.

Selection of ASAR Image Parameters in the CWAVE_ENV Model: Using the model given in (6), it is assumed that the n_s ASAR parameters include all relevant predictor variables. It is often required to select the variables such that no essential information is lost. On the other hand, too many variables will increase the computational effort as well as make the model rather sensitive to minor changes.

We choose ASAR parameters including the normalized radar cross section [(NRCS); referred to as well as $\sigma_\circ$, as shown in (7)], the variance of the normalized SAR image $cvar$ [29] [see (8)], and spectral parameters computed from the variance spectrum as essential variables in the CWAVE_ENV model to derive sea state parameters.

The NRCS of the SAR image is related to ocean surface wind based on the CMOD function [30], [31] and thus can represent short-wave information

$$\sigma_\circ = 10 * \log_{10}\langle I\rangle - K \tag{7}$$

$$cvar = \mathbf{var}\left((I - \langle I\rangle)/\langle I\rangle\right). \tag{8}$$

In (7) and (8), $\langle I\rangle$ is the mean intensity of ASAR wave mode data, and K is the calibration constant.

In the CWAVE_ENV model, 20 parameters are extracted from the estimated 2-D ASAR image spectra based on a set of orthonormal functions. Together with $\sigma_\circ$ and $cvar$, there are 22 ASAR image parameters that are collected into the vector $\mathbf{S}(s_1, \ldots, s_{ns})$ as input to model (6).

Estimation of the ASAR image spectrum is performed by computing the image periodogram with a 2-D FFT algorithm. This method implemented on the ASAR image spectral estimation is described in Appendix B. The exact definition of the orthonormal functions used to extract 20 ASAR image spectral parameters is given in Appendix C.

Although the exact physical meaning behind (6) is not easily interpreted, the 22 parameters include essential information relating the ASAR image to both long- and short-wave information, and therefore, the parametric model is successful in estimating ocean wave integral parameters of the complete wave spectrum.

B. Empirical Model Fitting Procedure

A least square minimization approach is used to tune the CWAVE_ENV empirical model as given by (9), where $(w^{(1)}, \mathbf{S}^{(1)}), \ldots, (w^{(N)}, \ldots, \mathbf{S}^{(N)})$ represents the available data pairs of ASAR image parameters and the collocated tuning data of integral wave parameters (e.g., SWH or mean wave period) derived from reanalysis WAMs or other observational data sources, which are treated as the "true" or, at least, very reliable sea state observations. It needs to be pointed out that different integrated wave parameters correspond to respective different parametric model coefficients

$$J_{\text{cost}}(\mathbf{A}) = \sum_{j=1}^{N}\left(w^{(j)} - \sum_{i=0}^{n_A-1}\mathbf{A}_i\mathbf{S}_i^j\right)^2. \tag{9}$$

As stepwise regression procedure is used for the least square minimization approach, the 22 parameters defined in the previous section are all included in the tuning approach; however, there are possibilities that some parameters will not lead to a significant improvement of the empirical model. To diagnose the performance on every ASAR image parameter collected in the vector $\mathbf{S}(s_1, \ldots, s_{ns})$, several terms are used to quantification.

The regression (or explained) sum of squares due to regression denoted RSS is

$$RSS = \sum_{j=1}^{N}\left(\sum_{i=0}^{n_A-1}A_i S_i^j - \overline{W}\right)^2. \tag{10}$$

The error (or residual) sum of squares ESS is

$$ESS = \sum_{j=1}^{N}\left(W_j - \sum_{i=0}^{n_A-1}A_i S_i^j\right)^2. \tag{11}$$

The multiple regression is performed on every ASAR parameter. The parameter S_{l1} for which RSS_{l1} is largest is chosen as the initial parameter. In the next step, a new parameter S_{l2} is selected, for which the incremental regression sum of squares RSS_{inc} is again the largest

$$RSS_{\text{inc}} = RSS_{l2} - RSS_{l1}. \tag{12}$$

In the third step, the testing of hypothesis that the inclusion of new ASAR parameter S_{l2} significantly reduces the regression sum of squares is performed by computing the test variable of

$$F^{(i+1)} = \frac{RSS_{\text{inc}}}{ESS_{l2}/(N-i)}. \tag{13}$$

This is compared to the critical value of the distribution $F(1, N-i)$ [28]. The iteration to select ASAR parameters will be terminated if the testing variable $F^{(i+1)}$ is below 0.99 or 99% quantiles, and the coefficients in (6) are fitted.

C. CWAVE_ENV Model Implementation

In the CWAVE_ENV empirical model, 22 parameters as introduced in the previous sector extracted from the ASAR wave mode image are used for the parametric model tuning approach.

The selection of a training data set for the empirical model is a crucial point. Its accuracy should be very near to the ground truth and be sufficiently representative of different sea states within the global geographical coverage.

In situ buoy measurements are believed to be the "ground truth (with 10% or 0.25-m accuracy for wave height)" and are used generally for assimilation into offshore WAMs, validation of global wave forecast models, and calibration and validation

of satellite wave sensors. Buoy measurements would be the best candidate for the tuning of the empirical model. However, the existing sea state reference buoys are limited in terms of global distribution and location (few are located in the open sea and in the Southern Hemisphere) [32].

The SAR/ASAR wave mode data are typically acquired globally in the open sea where only few buoy measurements are available. Therefore, in the present study, ASAR collocated ECMWF reanalysis WAM results in December 2006 are used as the tuning data set. As mentioned in Section II-B, the reanalysis ECMWF WAM is assimilated by satellite information. The data are publicly available, as well as reasonable tuning data set.

The histograms of SWH and T_{m02} derived from the collocated reanalysis ECMWF model spectra are shown in Fig. 3(a) and (b), respectively. It can be observed that the tuning data set includes different sea states. The dominant SWH ranges between 1.5 and 2.5 m, contributing around 50% to the entire tuning data set. The maximum SWH measured by the ECMWF model in the tuning data set is 12.6 m. The T_{m02} distribution shows that the model measures numerous waves with periods between 8 and 9 s, and long swell with periods larger than 12 s does exist in the tuning data set, too.

The coefficient vector $\mathbf{A}$ in (9) is thus tuned by using the ECMWF reanalysis WAM. Fig. 4 shows the goodness of fit on the optimization procedure in the CWAVE_ENV model based on the turning data set in December 2006. The left panel is for SWH, and T_{m02} is on the right one. The differences between ASAR measurements Y_i and observations X_i (numerical WAM or buoy) are quantified in terms of bias, rmse, and SI, which are expressed in the form of

$$\text{Bias} = \overline{Y_i} - \overline{X_i} \tag{14}$$

$$\text{rmse} = \sqrt{\frac{\sum (Y_i - X_i)^2}{n}} \tag{15}$$

$$\text{SI} = \frac{1}{\overline{X_i}} \sqrt{\frac{1}{n} \sum \left[\left(Y_i - \overline{Y_i}\right) - \left(X_i - \overline{X_i}\right) \right]^2}. \tag{16}$$

One can observe that the tuning approach of the CWAVE_ENV empirical model is successful, making the difference between ASAR measurements derived by the CWAVE_ENV algorithm and the ECMWF reanalysis model results in the tuning data set quite small with zero bias (as to be expected for the tuning), and low scatter indexes of 15% and 7% for SWH and T_{m02}, respectively. Thus, one can use the CWAVE_ENV geophysical model function (6) to derive sea state parameters from ASAR wave mode data.

IV. Assessment of the CWAVE_ENV Empirical Algorithm Performance

In this section, SWH, T_{m02}, and H_{12} derived from ASAR wave mode data are validated with *in situ* measurement comparisons, numerical WAM comparisons, and RA measurement comparisons on a data set different to the tuning data set.

H_{12} as given in (17) is associated with wave components with wavelength longer than 220 m, and such waves are directly detectable as patterns on the ASAR images

$$H_{12} = 4 \sqrt{\int_{f<1/12s} S(f) df}. \tag{17}$$

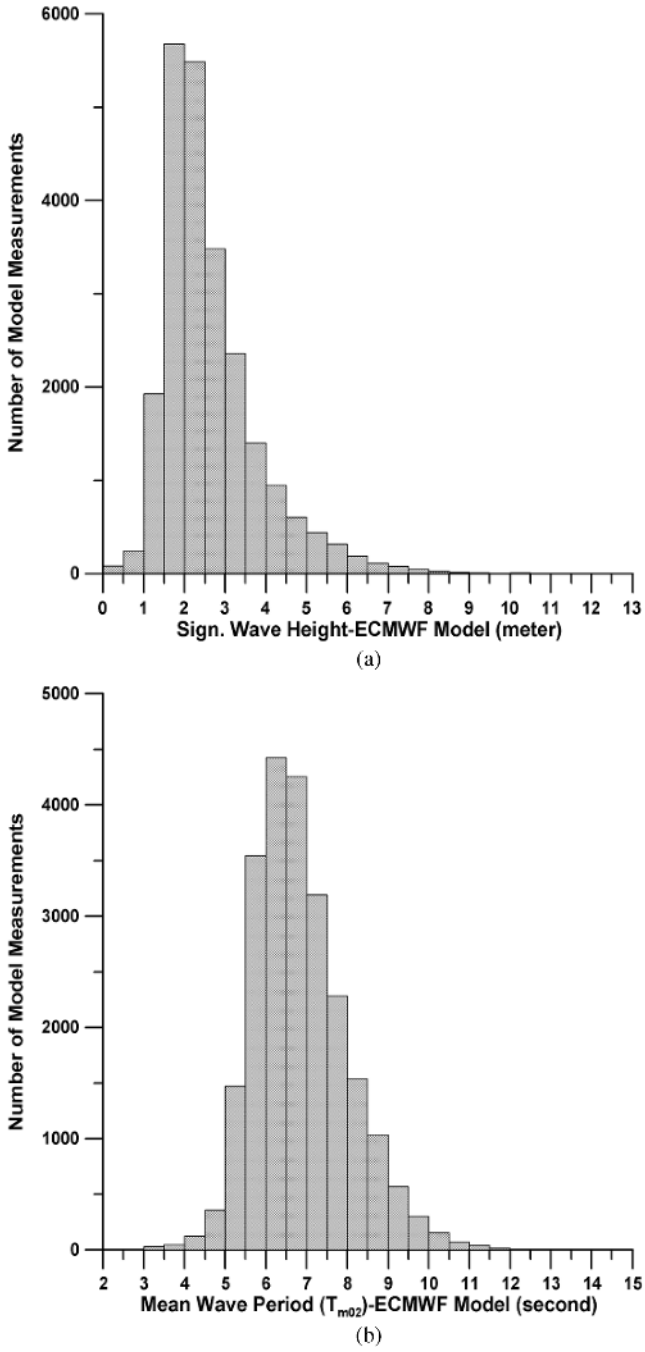

Fig. 3. Histograms of (a) SWH and (b) T_{m02} used in the tuning data set of the CWAVE_ENV model which are derived from the ECMWF-analyzed model in December 2006.

Validation results show that SWH relating to swell events (wave periods in the range of 10–15 s) as derived, e.g., from WAM operated in ECMWF has a positive bias larger than 0.25 m [23]. Such events are generated by storms in the Southern Hemisphere in winter season. Therefore, it is particularly interesting to compare wave height H_{12} derived

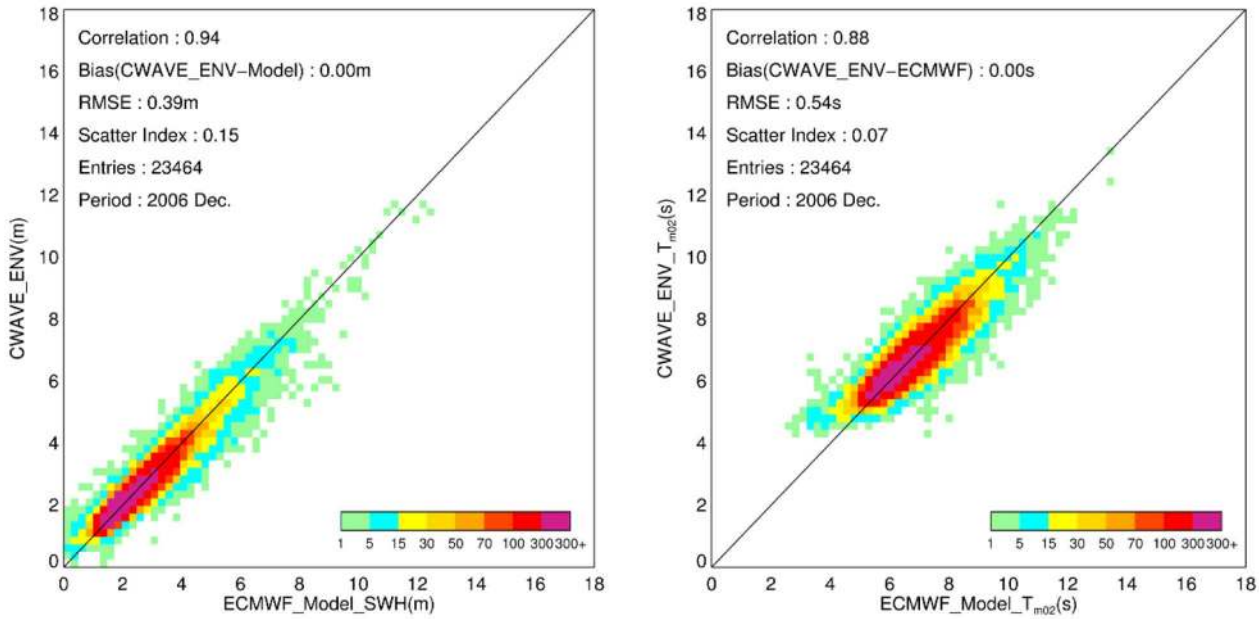

Fig. 4. Test of the goodness of fit for the optimization procedure in the CWAVE_ENV model based on the tuning data set in December 2006.

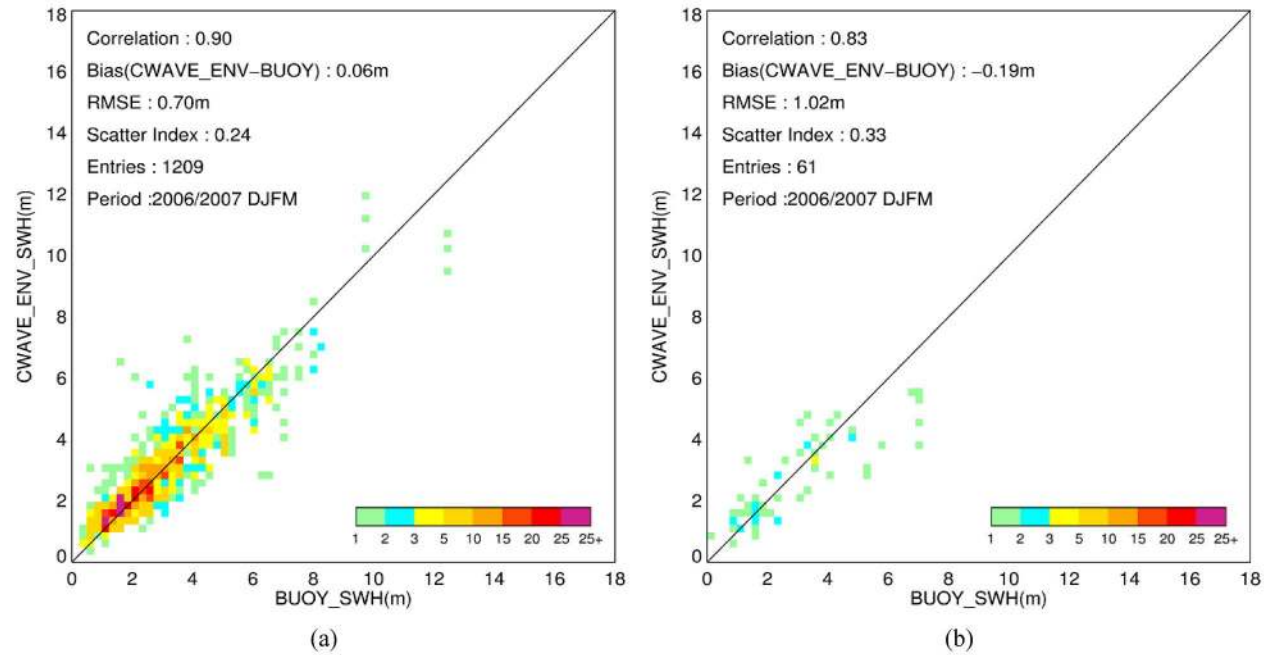

Fig. 5. Scatter plots of SWH derived by the CWAVE_ENV algorithm compared to buoy *in situ* measurements. Comparisons (a) in deep water and (b) in shallow water.

by the CWAVE_ENV algorithm to model results and SAR measurements such as the Level 2 product introduced by ESA.

A. Comparison to In Situ Data

Here, we present the validation of SWH derived by the CWAVE_ENV algorithm against *in situ* buoy measurements over the period in December 2006 and January, February, and May 2007. It should be pointed out that data pairs of ASAR imagettes and collocated buoy measurements in December 2006

TABLE I
STATISTICAL RESULTS DESCRIBING THE PERFORMANCE OF CWAVE_ENV FOR SWH (IN METERS) IN DIFFERENT SEA STATES

SWH (m)	Data Pairs	Bias (m)	BP (100%)	RMSE (m)	SI
(0,1.25]	170	0.45	47.6%	0.60	0.43
(1.25, 2.5]	456	0.20	10.0%	0.63	0.31
(2.5,4]	370	0.07	2.0%	0.69	0.21
(4,6]	208	-0.34	7.0%	0.77	0.14
>6	66	-0.91	12.6%	1.41	0.15

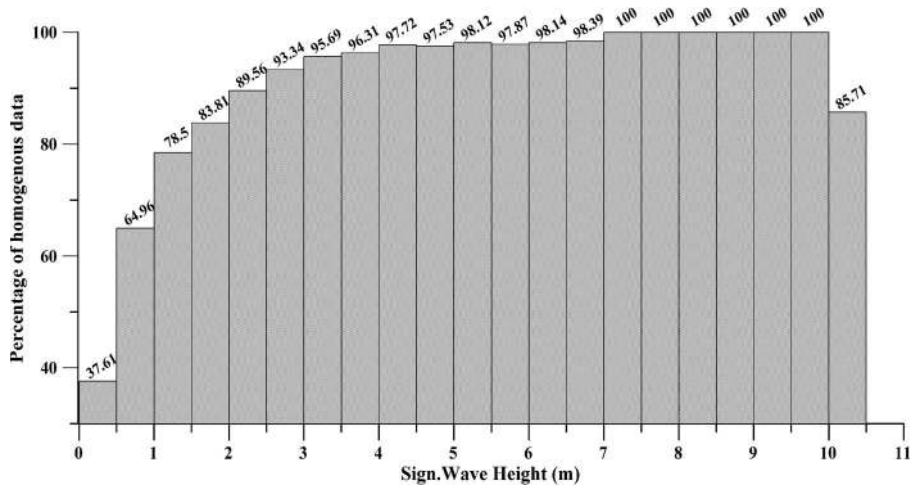

Fig. 6. Percentages of the ASAR wave mode data that pass the homogenous test in different sea states acquired during January–February 2007.

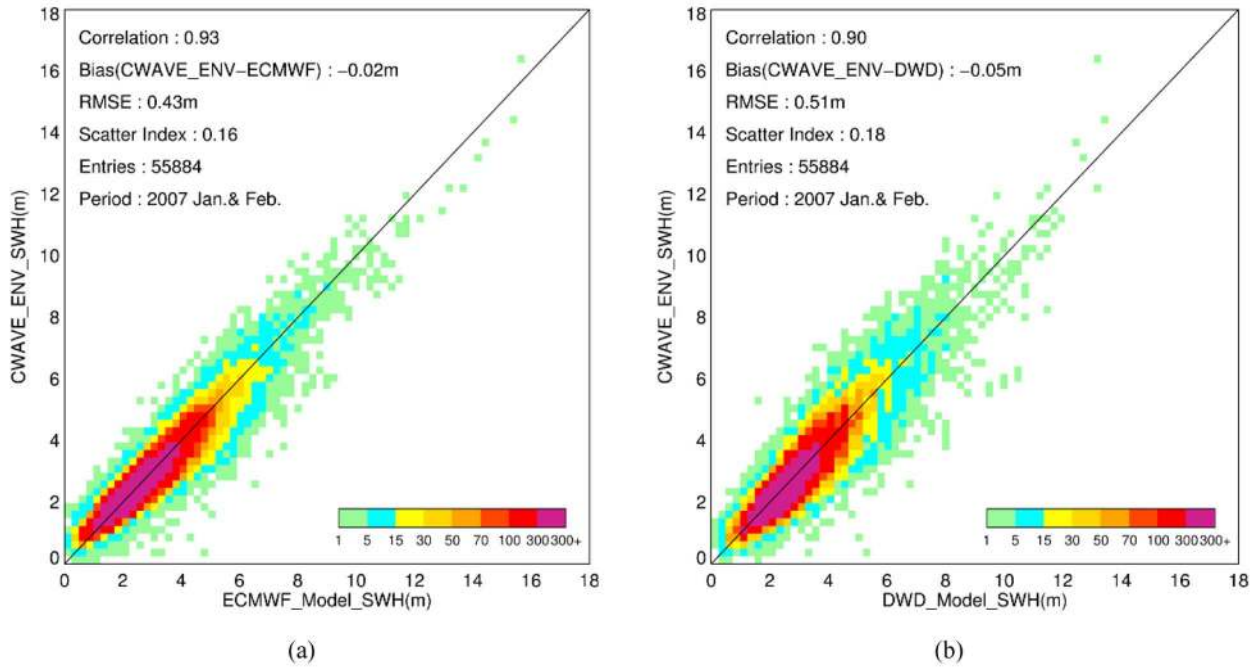

Fig. 7. Scatter plots of SWH derived by CWAVE_ENV compared to (a) the ECMWF reanalysis model and (b) the DWD forecast model for data acquired in January and February 2007.

were not included in the tuning data set. Buoy positions are shown in Fig. 2 and listed in Table IV of Appendix A.

The comparison is discriminated between deep water (depth $>$ 100 m) and shallow water cases, as shown in the scatter diagrams in Fig. 5(a) and (b), respectively. In deep water, SWH derived by the CWAVE_ENV empirical algorithm shows a good agreement against the buoy measurements.

One can observe that, generally, the empirical algorithm can provide reliable retrieved SWH from ASAR wave mode data with nearly zero bias, an rmse of 0.70 m, and an SI of 0.24 in deep water. Considering the 61 data pairs in shallow water, the retrieved SWH has a lower estimation with a bias of around 0.2 m, and the SI becomes rather higher to 0.33. As such, nearshore cases may be very variable and depend on collocation.

The tuning data set that we choose in the present study is the reanalysis numerical WAM, which has a good accuracy and global distribution and location. Taking into account the spatial resolution of the reanalysis WAM, the coastal ocean wave processes, e.g., wave shoaling and refraction induced by bathymetry, cannot be resolved though [33]. This therefore makes the retrieved results of CWAVE_ENV in shallow water show a high bias.

To investigate the performance of CWAVE_ENV for different sea states, i.e., from smooth to high sea state, a step comparison is carried out. In Table I, the results of the comparison are summarized. Aside from the three statistical parameters defined in Section III-B, the bias percent (BP) is used as well, estimating the relative bias depending on the mean value of buoy observations

$$\mathrm{BP} = 100\% * (\overline{Y_i} - \overline{X_i})/\overline{X_i}. \tag{18}$$

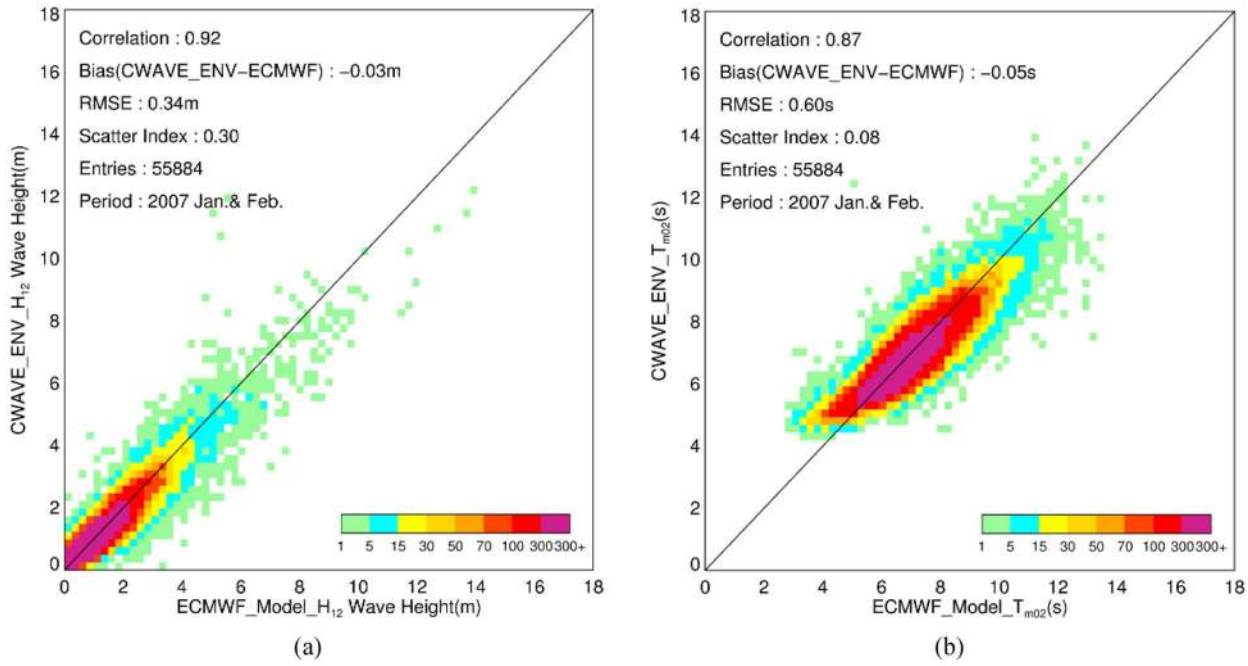

Fig. 8. Scatter plots of (a) wave height H_{12} and (b) T_{m02} derived by CWAVE_ENV compared to the ECMWF reanalysis model for data acquired in January and February 2007.

Considering the usual measurement for quality, namely, the SI, it is found that, in rough sea state, i.e., SWH $>$ 2.5 m, the CWAVE_ENV algorithm has a better performance with scatter indexes lower than 20%. In a sea state with SWH lower than 1.25 m, there is a distinct difference between CWAVE_ENV results and buoy measurements. Retrieved SWH is overestimated compared to the buoy measurements, and the SI in this sea state is 0.43. The distinct difference between radar and *in situ* buoy measurements in low sea state is also shown in the validation for the RA measurements as well, e.g., [35] and [37]. This somewhat is induced by the spatial inhomogeneity given by the fact that ASAR is sampling measurements every 100 km spatially while the buoy is averaged within 20 min.

In high sea state, namely, when SWH is higher than 4 m, SWH derived by CWAVE_ENV is underestimated compared to buoy measurements, and the bias increases with higher sea state. However, it is interesting to note that the SI is lower than 0.15, showing a quite promising agreement with *in situ* measurements in sea states with SWH larger than 6 m. Further investigation of the CWAVE_ENV algorithm will be considered for cases of very low ($<$ 1.0 m) and extreme sea state ($>$ 10.0 m) when compared to more collocations of *in situ* measurements.

In the next three sections, data pairs are collected in January and February 2007 for the comparisons to numerical WAMs, existing ASAR wave mode Level 2 WVW products, and the crossover RAs. Homogeneity tests are performed as well before the comparisons and validations. Fig. 6 shows percentages for the ASAR wave mode data that pass the homogeneity test in different sea states during the two months. One can observe that more than 60% data are excluded when SWH is lower than 0.5 m. When SWH is higher than 2.5 m, 90% data are homogenous and can be used for comparisons.

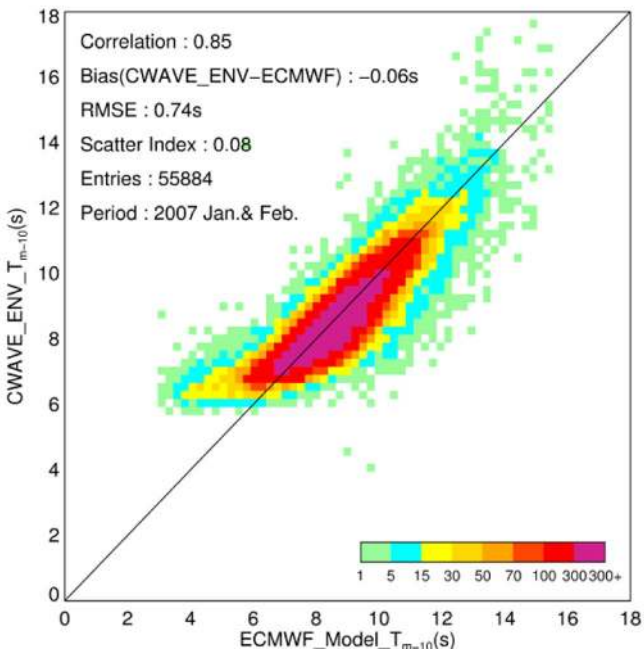

Fig. 9. Scatter plot of T_{m-10} derived by CWAVE_ENV compared to the ECMWF reanalysis model for data acquired in January and February 2007.

B. Comparisons to Numerical WAMs

In this section, SWH, H_{12} wave height, and T_{m02}, as well as wave energy period T_{m-10}, are compared to the ECMWF and DWD model results. The scatter plots in Fig. 7(a) and (b) show the SWH comparisons against the ECMWF and DWD WAM results, respectively.

Both plots in Fig. 7 show that SWH retrieved by the CWAVE_ENV empirical algorithm has good agreement

compared to the reanalysis and forecast models with zero bias, 0.43 and 0.51 m of rmse, and an SI of 0.16 and 0.18, respectively. For all statistical parameters, results derived from the CWAVE_ENV algorithm compared to the ECMWF reanalysis model have a better agreement compared to the DWD model. A plausible explanation is that the CWAVE_ENV algorithm is tuned by the ECMWF reanalysis model. In extreme sea state, e.g., when SWH is higher than 10 m, CWAVE_ENV results have a trend of slightly lower than the ECMWF model but higher than the DWD model.

As the ECMWF model has been assimilated with the *in situ* buoy and satellite data, thus, the DWD forecast results give more independent comparisons.

H_{12} and T_{m02} measurements are not available for the model provided by DWD. Results derived from the CWAVE_ENV algorithm for these parameters are compared to the ECMWF reanalysis model, as shown in Fig. 8(a) and (b). The SI of the H_{12} comparison is 0.3, while the bias still remains very low at 3 cm. T_{m02} comparison has an SI of 0.08, and the rmse is 0.6 s.

In addition to SWH, wave energy period $T_{m-10} = m_{-1}/m_0$ is another key parameter and is used to calculate the wave power J via

$$J = 0.49 H_s^2 T_{m-10} \tag{19}$$

where J has units in kilowatts per meter [36]. The wave energy period is also retrieved by the CWAVE_ENV algorithm and compared to the reanalysis ECMWF model, as shown in Fig. 9. As ASAR images are typically requested as well for other modes (e.g., image mode with 100 km by 100 km swath coverage), which is exclusive to wave mode in offshore regions, we are following the idea of extending the CWAVE_ENV algorithm to image swath ASAR data to retrieve sea state parameters. Thus, coastal wave power statistics will become available. This is interesting for many coastal applications.

In Table II, the statistics of the comparisons to both WAMs are summarized. Integral wave parameters given by CWAVE_ENV have nearly zero bias when compared to models. T_{m02} has the smaller SI of 0.08, while it has the highest bias of -0.05 s and an rmse of 0.59 s in the triple comparisons.

C. Comparison to ASAR Wave Mode Level 2 Products

For the Envisat mission, ESA delivers the ocean wave spectra of Level 2 products WVW to the users. The data are provided on a log-polar grid with 24 wavelengths and 36 directions. In this section, WVW product performance is compared to the result of the CWAVE_ENV algorithm for SWH and H_{12}. Fig. 10 shows the two comparisons for different wave heights of SWH and H_{12} as derived from ESA WVW product retrievals and the CWAVE_ENV algorithm. For SWH lower than 4 m, the WVW products are generally suitable for providing sea state measurements although, in many cases, cannot yield a successful spectrum retrieval (as shown by the numerous entries in the Y-axis with zero value of WVW results). When sea state is higher than 4 m, a systematic underestimation of wave height estimated from WVW products is quite obvious.

It is no surprise that the algorithm is limited to retrieve long-wave information contained in the SAR image. Even if it is argued that the WVW spectrum results are only available for the longer wave information resolved by the ASAR sensor, it still cannot provide reliable sea state measurements in many swell cases as shown for the H_{12} wave height comparison, which are, in fact, the results for waves already longer than 220 m.

D. Comparison to RAs

As mentioned in Section I, RA is another radar remote sensing instrument that can provide accurate SWH measurements over the sea surface. In this section, cross validation of SWH retrieved by CWAVE_ENV is carried out. Measurements acquired from the JASON-1 and GFO missions during January–February 2007 are used. The data are acquired via the Center for Satellite Exploitation and Research (CERSAT) database, and the corrected SWH is used. For JASON-1, the corrected result is $SWH\_corr = 1.0429 * SWH + 0.0266$, and for GFO, the respective equation is $SWH\_corr = 1.0625 * SWH + 0.0754$ [3].

We choose the time window for ASAR wave mode data collocated to RA to be 1 h and the distance of collocation to be smaller than 100 km. The crossover sea state measurements derived from GFO and JASON-1 are fully independent for the retrieved SWH from ASAR data. Within an area with a radius of 100 km, several RA single-point measurements are collocated to the ASAR wave mode data. Therefore, the averaged SWH within the collocation cells and the single SWH from the nearest point are both compared to the result derived by CWAVE_ENV from the ASAR wave mode data. Figs. 11 and 12 show the retrieved SWH compared to GFO and JASON-1, respectively.

One can observe that all the comparisons are in very close agreement. The overall bias is around 0.10 m, and the rmse is around 0.50 m. The correlation is higher than 90%, and the scatter indexes are 0.17 and 0.13 for comparisons to GFO and JASON-1, respectively. Thus, the SWHs derived by the empirical model from ASAR data and altimeter measurements are of the same quality.

In this section, sea state parameters retrieved by CWAVE_ENV algorithms are compared to different data sets. The comparisons show that the integral wave parameters derived from ASAR wave mode data are reliable and independent. It can be used as another data set for global wave statistical analysis.

V. Global Wave Parameter Statistics

Knowledge of the global behavior climate of ocean surface waves, in terms of seasonal patterns and natural variability, is of central importance to climate studies. The information used to study wave climatology comes mainly from two sources: 1) direct wave measurements and observations and 2) hindcast with WAMs. *In situ* measurements using wave buoys and shipborne wave recorders, as well as visual inspections from vessels participating in the voluntary observing ship scheme, are the traditional data source for wave observations. Using the visual wave data along the major ship routes covering the period from 1958 to 1997, the climatology of swell and wind sea in global scale is derived [37].

TABLE II
STATISTICS OBTAINED BY THE CWAVE_ENV ALGORITHM VERSUS THE ECMWF MODEL AND THE DWD MODEL FOR SWH (IN METERS), H_{12} WAVE HEIGHT (IN METERS), T_{m02} (IN SECONDS), AND T_{m-10} (IN SECONDS) IN JANUARY AND FEBRUARY 2007. BIAS IS WITH RESPECT TO OBSERVATIONS, AND SI INDICATES SCATTER INDEX

	CWAVE_ENV vs. ECMWF model				CWAVE_ENV vs. DWD model			
Statistical Para.	Cor.	Bias	RMSE	SI	Cor.	Bias	RMSE	SI
SWH	0.93	-0.02 m	0.43 m	0.16	0.90	-0.05m	0.51m	0.18
H_{12}	0.92	-0.03 m	0.34 m	0.30		N/A		
T_{m02}	0.87	-0.05 s	0.60 s	0.08		N/A		
T_{m-10}	0.85	-0.06 s	0.74 s	0.08		N/A		

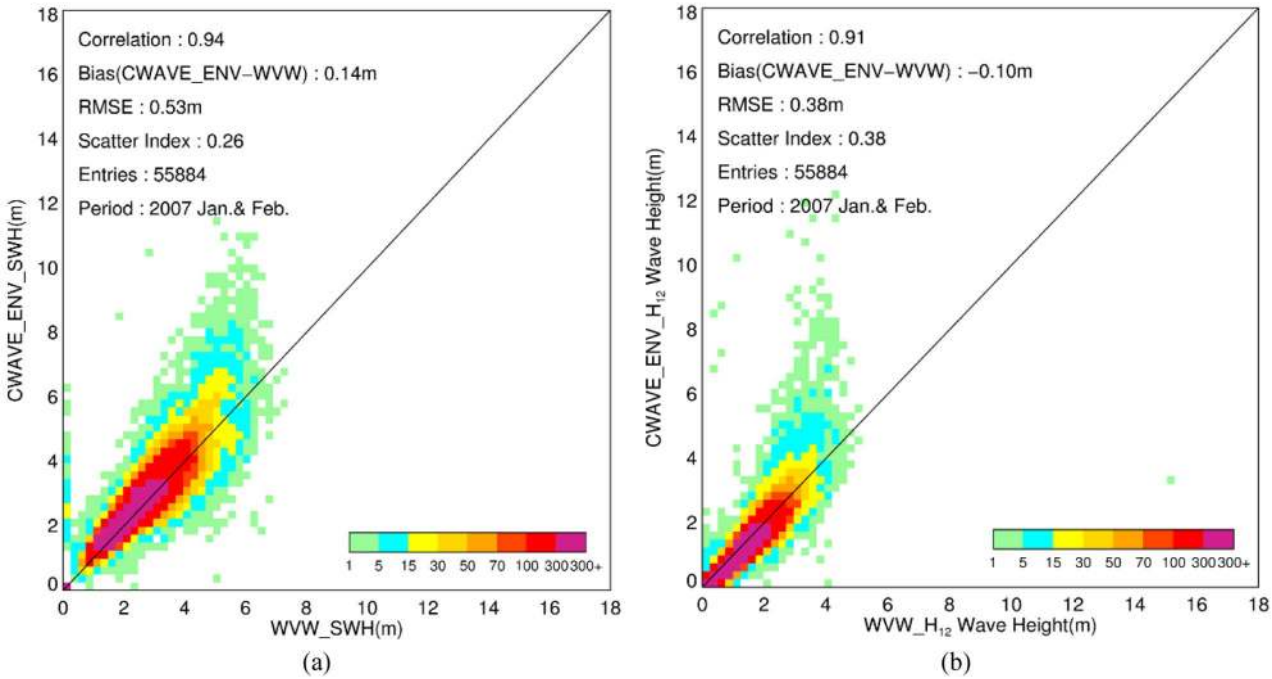

Fig. 10. Scatter plots of (a) SWH and (b) H_{12} derived from ESA WVW spectra compared to CWAVE_ENV algorithm results for data acquired in January and February 2007.

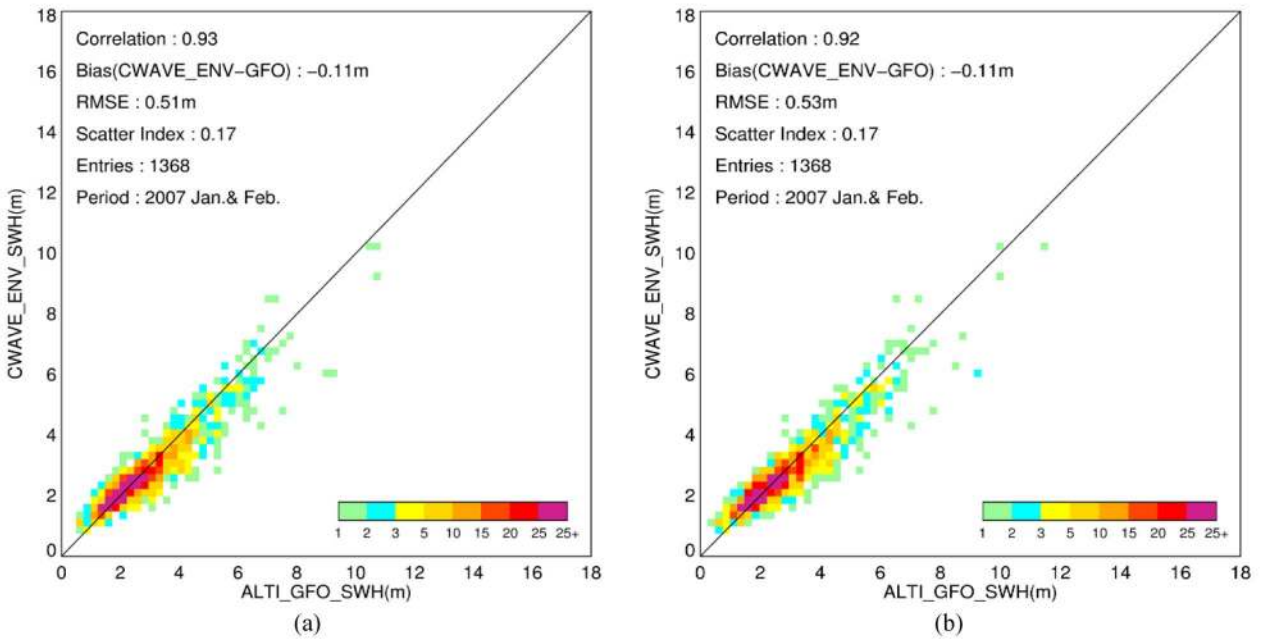

Fig. 11. Scatter plots of SWH derived by CWAVE_ENV compared to the measurements of RA GFO. (a) Comparison to the averaged SWH within the collocation cells. (b) Comparison for the single SWH of the nearest point to ASAR wave mode data.

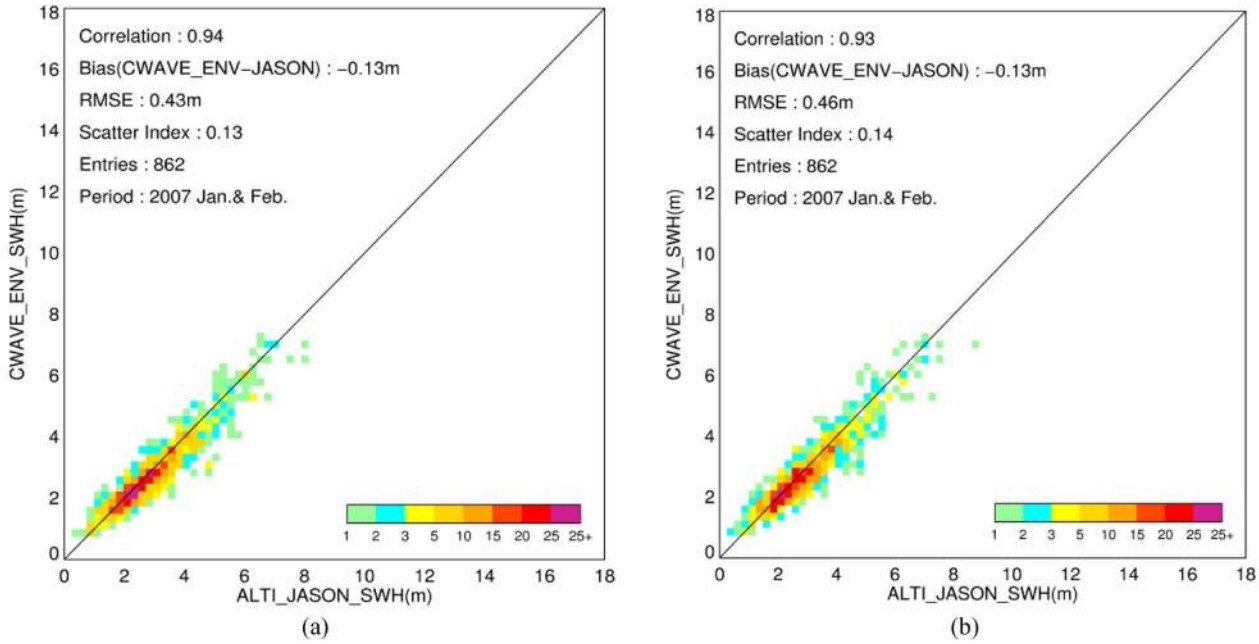

Fig. 12. Scatter plots of SWH derived by CWAVE_ENV compared to the measurements of RA JASON-1. (a) Comparison to the averaged SWH within the collocation cells. (b) Comparison for the single SWH of the nearest point to ASAR wave mode data.

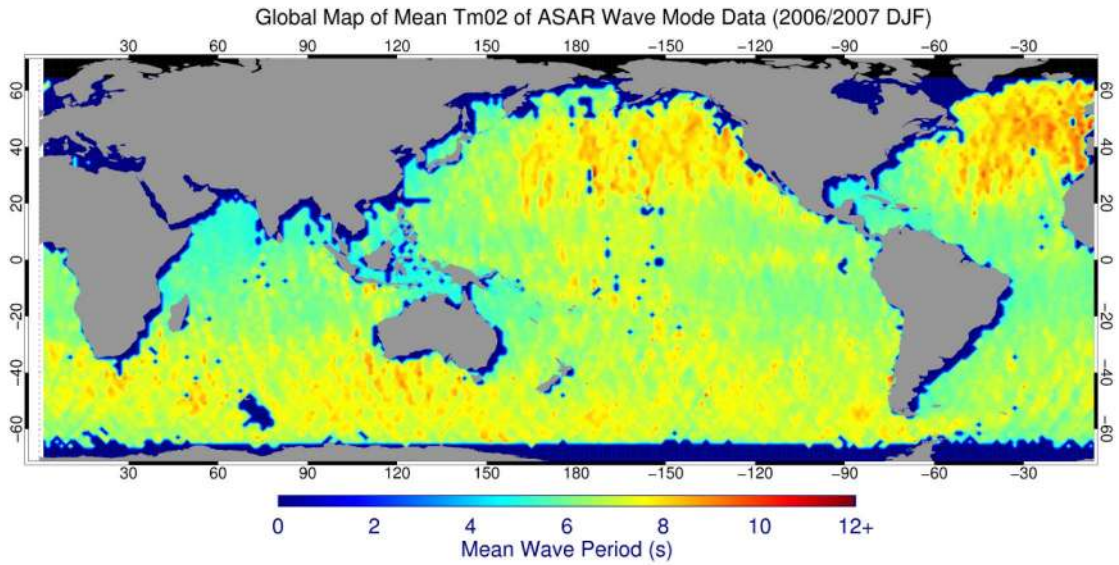

Fig. 13. Mean SWH in 1.5° by 1.5° boxes derived from ASAR wave mode measurements.

Numerical WAMs are playing an important role in wave climatology analyses. Numerous wave climatology studies, particularly regional climatology, are based on numerical WAM hindcast or reanalysis data set, e.g., using the three WAM data sets spanning 40 years, i.e., ERA-40 [25], WASA [38], and ODGP2 [39]. In general, all of these studies show similar wave climate changes, e.g., compared to research by Sterl and Caires [40], a trend in 99-percentile SWH of about 7 cm/year was also found in the North Atlantic in the study of Wang and Swail [39]. Another highlight of this 40-year analysis of ODGP2 adds convincing support to the WASA group's conclusion that "the northeast North Atlantic has indeed roughened in recent decades, but the present intensity of the wave climate seems to be comparable with that at the beginning of this century." Satellite remote sensing, particularly from RA and SAR, as well contributes to global wave climate analysis, although the time span still only covers about 20 years. Concentrated on the combined monthly gridded data set from ERS-1, ERS-2, and TOPEX that provides continuous coverage of the period August 1991–February 2000, the pattern with the highest interannual variability, similar to the North Atlantic oscillation, was found by Woolf *et al.* [41]. Using three years of reprocessed ERS-2 SAR wave mode data, global and zonal mean SWH variability is derived by König *et al.* [42].

Here, global maps of mean SWH and T_{m02} derived from ASAR wave mode data are presented for the three-month

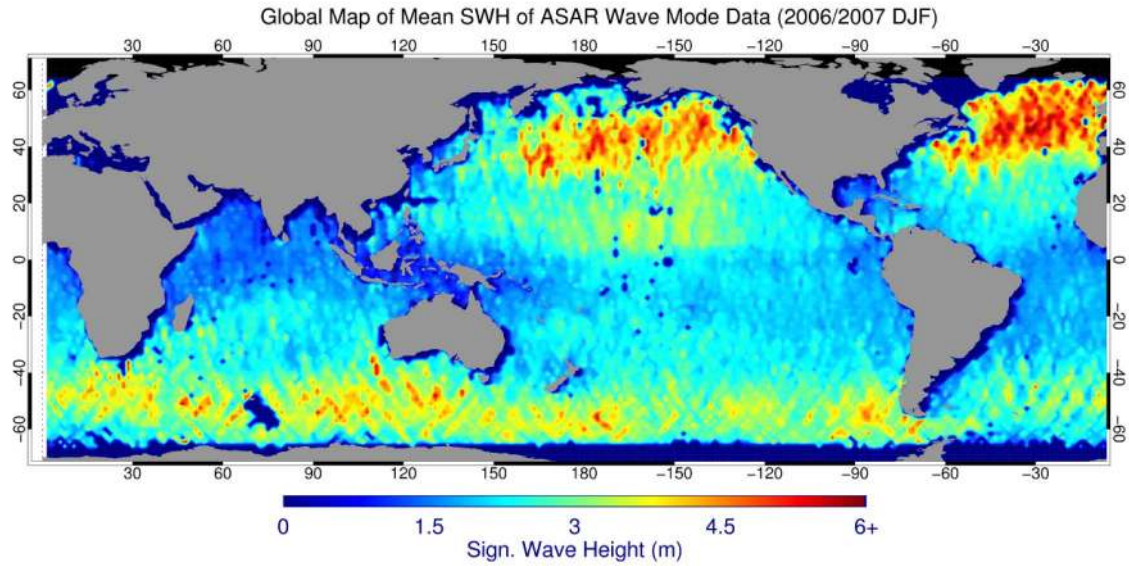

Fig. 14. Mean energy wave period in 1.5° by 1.5° boxes derived from ASAR wave mode measurements.

period of December 2006–February 2007. It is used as demonstration for a compilation of a global wave statistical analysis.

A. SWH

In Fig. 13, the global map of SWH retrieved by the CWAVE_ENV algorithm from ASAR wave mode data is shown. In some coastal regions, where the antenna stations regularly acquire data in other modes (e.g., image mode with a swath of 100 km by 100 km), wave mode data are not available, and together with the wave mode acquired in both polar regions, they are indicated black areas on the map.

It is obvious that, in the North Atlantic and North Pacific, mean SWH is higher than that in all other ocean basins. In particular, in the area between 40° N to 60° N and 0° W to 50° W, winter storms often lead to mean SWH higher than 5 m.

B. Mean Wave Period

A global map of mean wave period is compiled and shown in Fig. 14. In the North Central Pacific, features of the distribution of wave period are similar to the one for SWH shown in Fig. 13.

In the north, high waves with average SWH above 5 m almost cover the entire region between 40° N and 60° N. Mean wave period builds up continuously toward the east. This shows that the North Atlantic is a fetch-limited basin with steeper waves toward the west. Storm systems of high forward speed generate high waves, which often are not fully developed.

The two global maps are compiled based on three months of data, which is too short to derive global wave statistical properties. Further investigation using the CWAVE_ENV empirical algorithm to derive the sea state statistics will be spanning the entire era of Envisat mission. In principle, the ERS data have been available since 1991.

VI. Case Studies

Two case studies are investigated in this section, namely, a severe storm that occurred over the North Atlantic on February 10, 2007, and the La Reunion extreme swell event, which was generated by a distant storm in the south of Cape Town, South Africa. Both cases are analyzed using WAM outputs and double tracks of ASAR and RA-2 onboard the Envisat satellite. With respect to the storm case, performances of different SAR retrieval algorithms in extreme wind speed and sea state are compared to WAM results. In the La Reunion case study, we investigate ASAR measurements over a storm, which generated high swell across the entire Indian Ocean basin. Based on the empirical swell propagation law, the capability of ASAR wave mode data to be used for early warning systems is analyzed as well.

A. North Atlantic Storm Event

In this section, a North Atlantic storm event is investigated in detail by using ASAR wave mode data, RA data, and DWD forecast WAM results. Fig. 15 shows radar measurements and WAM results for the event. In (a) and (c) in the figure, SWHs of the DWD forecast model results at 00:00 and 12:00 UTC are shown as the background, on which collocated SWH measurements from the double tracks of ASAR and RA-2 are superimposed. ASAR provides sea surface measurements in right-looking mode; thus, its surface track is around 300 km away from the nadir measurements of RA-2. At 00:00 UTC, the eastern track is the one of ASAR. Due to ascending and descending orbits, it becomes the western track in the descending case at about 12:00 UTC.

SWH derived from radar measurements and model forecast results through the western high-wave system is analyzed in the following. SWHs derived from ASAR and RA-2 data along the tracks are represented by different curves in Fig. 15(b) and (d) for 00:00 and 12:00 UTC. For SWH retrieved by the ASAR algorithms, estimation by using the CWAVE_ENV algorithm is shown in blue line; the nonlinear retrieval algorithm PARSA and the Level 2 WVW products are shown in brown and yellow ones, respectively. The DWD model results collocated with the ASAR track are plotted as well as a pink line. Estimation of

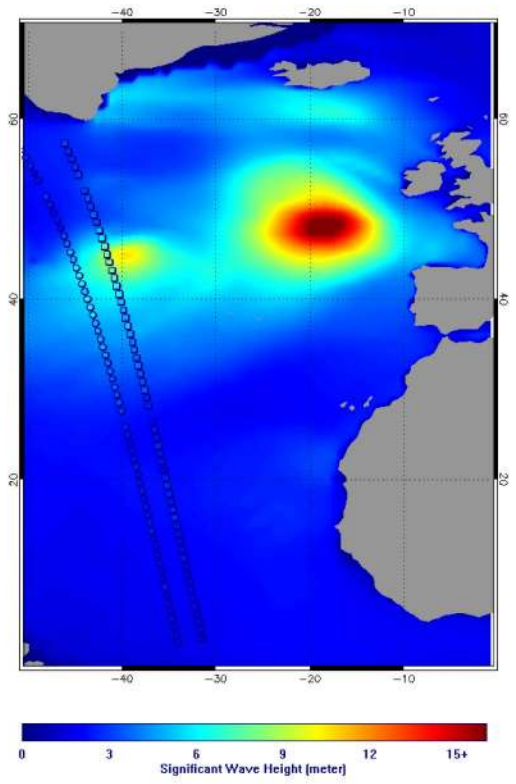

(a)

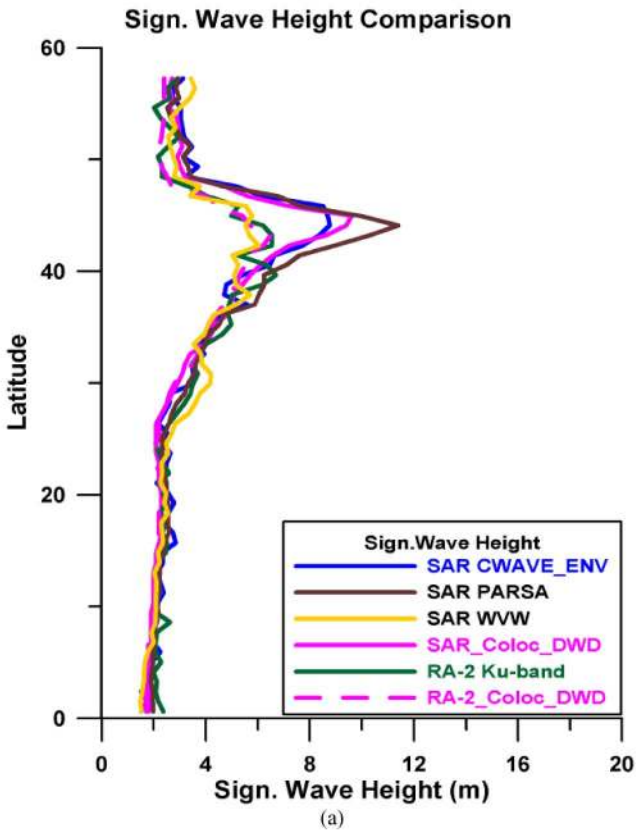

(a)

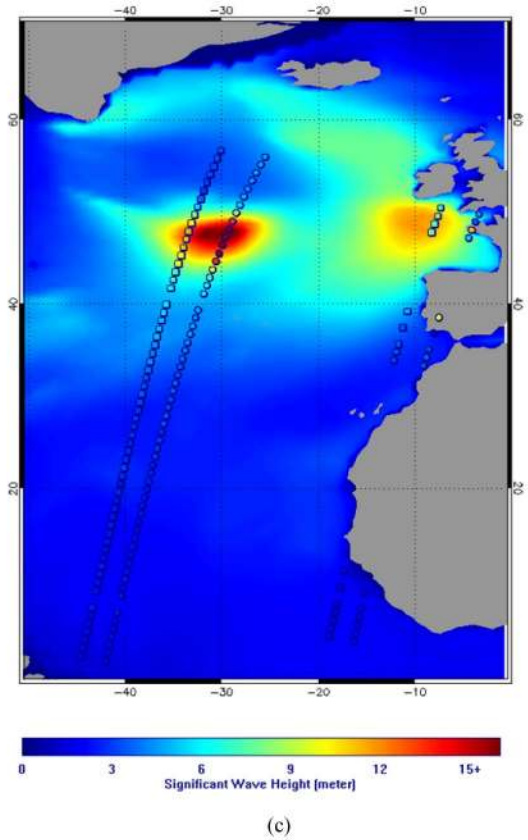

(c)

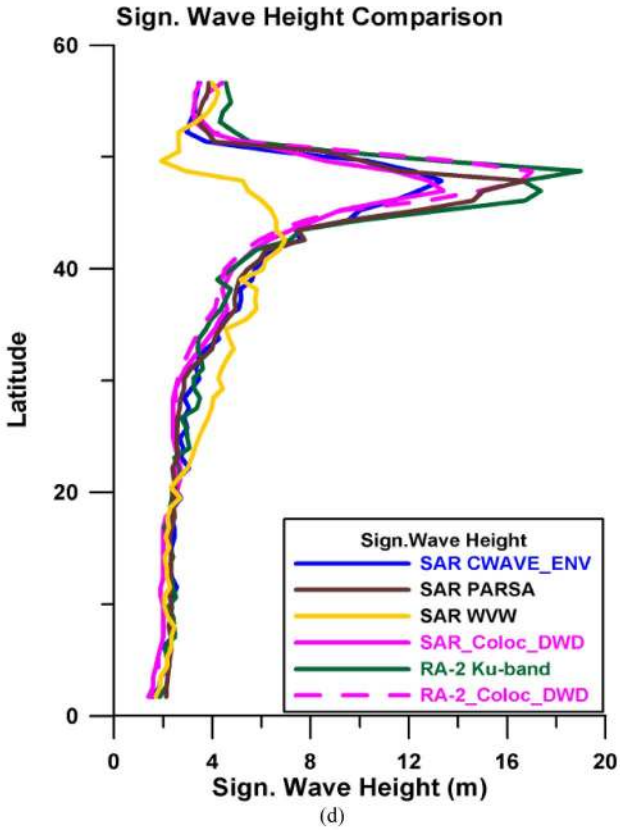

(d)

Fig. 15. Comparison of SWH derived from the DWD forecast model, ASAR wave mode data, and RA-2 data for the North Atlantic storm on February 10, 2007. (a) DWD forecast model at 00:00 UTC superimposed with ASAR (eastern) and RA-2 tracks. (b) SWH derived from ASAR track using different algorithms, RA-2, and the collocated DWD model results at 00:00 UTC. (c) Same with (a) while at 12:00 UTC. (d) Same with (b) while corresponding to the tracks acquired at 12:00 UTC.

TABLE III
AVERAGED SWH ESTIMATED FROM DIFFERENT ASAR ALGORITHMS AND DWD MODEL RESULTS IN THE HIGHER WAVE FIELD FOR ASCENDING AND DESCENDING PASSES

	CWAVE_ENV	PARSA	WVW	DWD model
Ascending Pass (at about 0:20 UTC)	8.5 m	9.6 m	5.7 m	8.4 m
Descending Pass (at about 0:20 UTC)	10.9 m	11.4 m	5.1 m	10.2 m

SWH derived from the RA-2 K_u-band is also used for comparison. It is represented by green lines in the plot, and pink dashed lines are used to denote its collocated DWD model results. As RA-2 has the nadir footprints which are 300 km away from the ASAR measurements, the WAM results collocated to RA-2 are different to the ones for the ASAR track.

Both curve plots show that SWH derived from ASAR wave mode data and RA-2 has quite good agreement with wave forecast model results when sea state is lower than 6 m. In high sea state, the differences are quite obvious though. At 00:00 UTC, the ASAR track is crossing the area of the wave system, yielding high SWH. The PARSA algorithm provides the highest value of 11.4 m, while the WVW product has a large underestimation and yields only 5.7 m. The differences of using the ASAR algorithms to estimate SWH in high sea state are investigated in detail as follows.

ASAR wave mode data are acquired along the orbit every 100 km to provide sample and instantaneous measurement over sea surface. To avoid high variations for SWH estimation using ASAR wave mode data in high sea state, an averaging way is used. In the ascending pass of Envisat at around 00:15 UTC, five data pairs of ASAR measurements and collocated DWD model located in the region between 42.32° N and 45.85° N which is near to the high-wave system are linear averaged, avoiding the effect of sampling of ASAR measurements. In the descending pass at around 12:40 UTC, the area is chosen to be between 43.47° N and 49.63° N, where eight data pairs are located with all wave heights higher than 7.0 m.

The averaged SWH measurements derived from different algorithms and collocated DWD model results for both tracks are given in Table III.

For both tracks, the CWAVE_ENV algorithm shows the capability to derive reliable measurements even in this extreme sea state, while the WVW products cannot be used to measure high sea state. Even when the SWH is lower than 5 m, the WVW products have a positive bias compared to other algorithms and model results, which is particularly obvious in the descending pass as shown with the yellow line in Fig. 14(d). Therefore, from this case study, one can conclude that WVW has a substantial underestimation in high sea state and rather overestimation in low and moderate sea states.

The PARSA algorithm yields higher estimation of SWH in both tracks than the DWD WAM and the CWAVE_ENV results. Moreover, the positive bias increases significantly along with the sea state. The PARSA algorithm is implemented using the prior information from the ECMWF reanalysis WAM, in which the ASAR wave mode cross-spectral information and RA measurements have been assimilated. The PARSA algorithm might have an overestimation due to instantaneous measurements in comparison to averaged model results. This needs to be further validated.

At around 12:35 UTC, the RA-2 track was very near to the high-wave system and yields an estimation of SWH of 18.9 m, which is 2.9 m higher than the DWD model forecast result. For this high sea state, the performance of different ASAR algorithms to derive SWH is investigated in detail, particularly to evaluate the CWAVE_ENV algorithm and the existing WVW Level 2 products. CWAVE_ENV results for both passes show reliable measurements of SWH in different and variable sea states.

This case study shows that the quality of retrieved sea state parameters by CWAVE_ENV is comparable to RA measurements and to the SAR nonlinear retrieval approach, although no prior information is used. The double tracks of ASAR and RA can be used jointly to validate the WAM performance, as well as for data assimilation, under the condition that a suitable algorithm for ASAR is adopted. With respect to the CWAVE_ENV algorithm, one issue that needs to be further investigated is the performance in extreme sea state for extended data sets.

B. Indian Ocean Swell Case

On the evening of May 12, 2007, a series of very high waves damaged the coasts of La Reunion island (21° S, 55°20′ E) and neighboring islands in the Indian Ocean. The extreme swell with a peak period of up to 19.5 s reached a maximum individual height of 11.3 m and an SWH of 6.4 m [43].

The extreme swell is generated by a severe storm around 40° S, 30° E in the south of Africa, as shown in Fig. 16, with wind (upper panel) and wave field (lower panel) given by the DWD forecast model on May 10, 2007, at 06:00 UTC. The storm engendered swell, which propagated through the Indian Ocean covering about 1000 km/day, hitting La Reunion.

Early Warning of Extreme Wave Using ASAR Wave Mode Data: In Fig. 17, SWH measurements derived from both tracks of ASAR wave mode data using the CWAVE_ENV algorithm and RA-2 data are superimposed on collocated DWD forecast model results. The time difference between the Envisat track and the DWD model is around 1.5 h.

Compared to Fig. 16, one can observe that the storm was moving toward northeast and spanned quite a large region of more than 1000 km. The Envisat tracks cross the area of the storm at around 19:45 UTC on May 11. The highest SWH measured along the ASAR track is 9.2 m located at 32.2° S, 4.7° E. A high-swell system traveled to the northeast and arrived at La Reunion island on May 12 at around 16:00 UTC after traveling 1700–2000 km. Using straightforward wave propagation relationships introduced by Dietrich *et al.* [44], about 5-m waves can be forecasted in La Reunion island at around 12:00–16:00 UTC on May 12. This shows good agreement with the *in situ* and reanalysis model, which yields 6 m [43].

In this case, around 20 h earlier, the extreme swell arriving at La Reunion island can be forecasted by ASAR wave mode measurements derived from the CWAVE_ENV algorithm. The

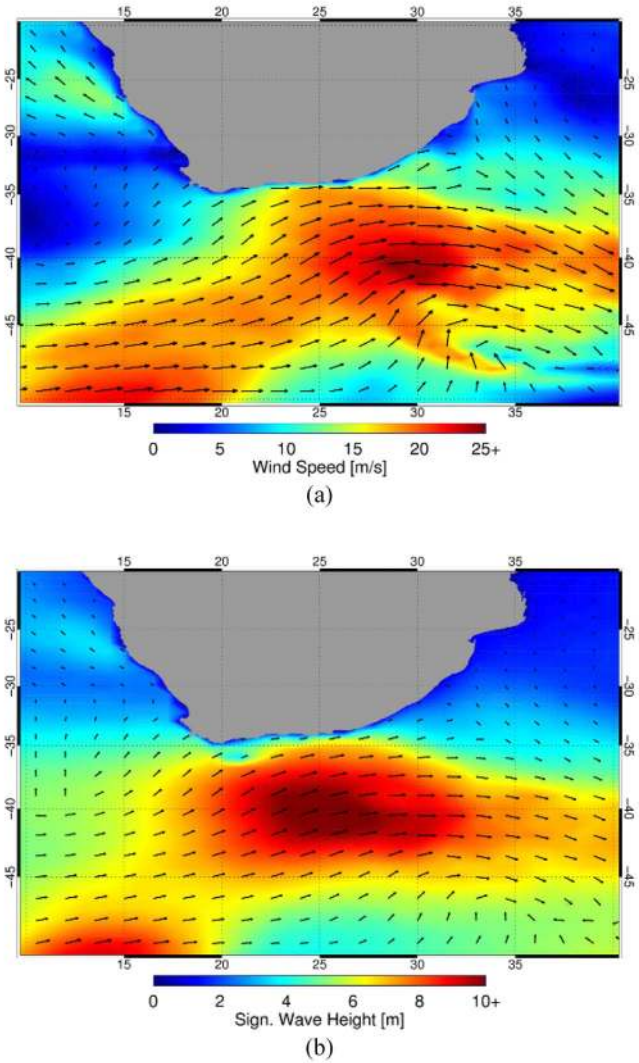

Fig. 16. (a) Wind field and (b) SWH with direction of wind sea of the DWD forecast model on May 11, 2007, at 06:00 UTC.

ASAR wave mode data may also be used together to cross validate; thus, an extreme-wave early warning system is possible.

VII. Conclusion and Discussion

An empirical algorithm referred to as CWAVE_ENV to estimate integral wave parameters from ASAR wave mode data without prior information has been presented in this paper. The empirical model function is tuned using globally distributed ASAR wave mode data and collocated ECMWF reanalysis model results. The tuning approach is implemented using a stepwise regression method to select ASAR image parameters. The geophysical model coefficients are derived by cost function minimization.

Validation of the CWAVE_ENV algorithm is carried out by comparison against *in situ* measurements, numerical WAMs, Envisat/ASAR Level 2 WVW products, and crossover RA measurements. Validation results show that the accuracy of integral wave parameters retrieved by the CWAVE_ENV algorithm has the quality of the RA measurements and is near to *in situ* buoy

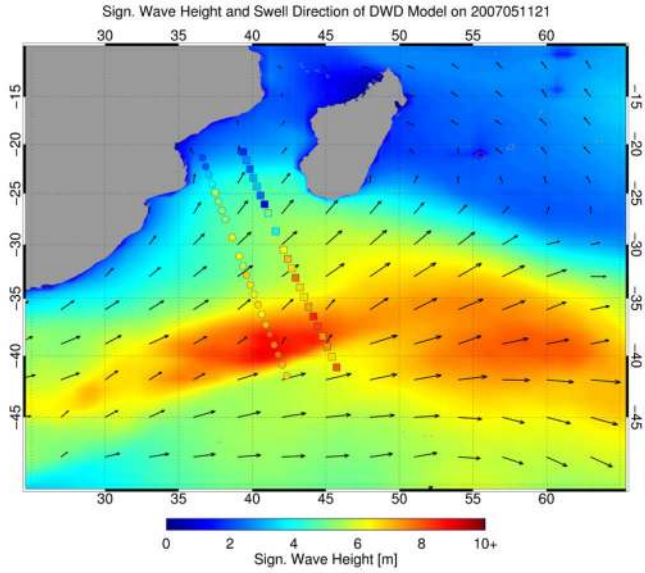

Fig. 17. SWH and swell direction of the DWD model on May 11, 2007, at 21:00 UTC. The double tracks of (squares) ASAR wave mode and (circles) RA-2 at around 19:45 UTC are superimposed.

measurements. A brief summary of the algorithm validation is given in the following.

1) SWHs retrieved from ASAR data compared to buoy *in situ* measurements are divided into comparisons in deep water and shallow water. In deep water, retrieved SWH has a good correlation of 0.9 to buoy measurements, a reasonable rmse of 0.70 m, and an SI of 0.24. The comparison in shallow water yields rather high rmse of 1.0 m and an SI of 0.33 m, due to the limitation of the reanalysis WAM data in the empirical model tuning.

   Investigating the comparison of the CWAVE_ENV algorithm in different sea states demonstrates that the algorithm has good performance in rough sea state (with SWH higher than 2.0 m), while it has an overestimation around half meter in the rather low sea state for SWH less than 1.25 m.
2) SWH, H_{12} wave height, and T_{m02} compared to the ECMWF reanalysis models are also presented. CWAVE_ENV results have a low bias of -0.02 and -0.03 m for SWH and H_{12} and an rmse of 0.43 and 0.34 m, respectively, while the wave period comparisons show a very low SI of 8%.

   As the DWD WAM is independent of ASAR information, comparison of SWH estimated by CWAVE_ENV to the DWD WAM, with a small bias of -0.05 m and an SI of 0.18, shows more realistic results than the comparison to the ECMWF reanalysis WAMs, which is using the *in situ* measurements and satellite data in the assimilation scheme.
3) The retrieved results of SWH and H_{12} by CWAVE_ENV are also compared to the ASAR wave mode Level 2 products. The comparison results reveal that the existing Level 2 products significantly underestimate SWH, and the measurements vary with the change of ASAR cutoff wavelength.

4) RA measurements are also used for the validation of the CWAVE_ENV algorithm. Crossover measurements from the GFO and JASON-1 missions are collocated to the ASAR wave mode data. A bias of around -0.1 m and an rmse of around 0.5 m are found for both comparisons. Low scatter indexes of 0.13 and 0.17 are achieved when compared to GFO and JASON-1, respectively. Few cases over extreme sea state with an SWH of around 10 m have consistent results from the ASAR wave mode and GFO data.

The results of the two case studies for extreme wave conditions thus demonstrate that the CWAVE_ENV algorithm performs well under extreme sea states.

In the North Atlantic storm event case, the SWHs given by ASAR and RA-2 are compared to the DWD forecast WAM. All measurements derived from radar and models agree well along the orbit, but for the extremely high sea state within the storm, there are distinct differences. CWAVE_ENV results agree well with the DWD model results but are around half meter higher for SWH above 7 m. Both RA-2 and ASAR PARSA results are higher than the wave forecast with a bias of more than 1 m in extreme sea state. The ASAR standard Level 2 WVW products show a significant underestimation of wave height in storm areas.

The analysis of the high-swell case at La Reunion island demonstrated that ASAR wave mode data can be used as a forecasting tool for extreme waves contributing to a global early warning system.

Despite the overall good quality of integral wave parameters derived by the CWAVE_ENV algorithm, the assessment is based on a three-month period. Therefore, a more intensive validation by *in situ* buoy measurements and crossover RA measurements is needed to confirm its performance under extreme sea state conditions.

In the present study, coefficients in the CWAVE_ENV model are tuned by the reanalysis ECMWF WAM, in which available wave observations have been assimilated. This, to some extent, limits the current results to be used fully independent. However, the empirical algorithm demonstrates that the integral wave parameters can be retrieved correctly, even without using *a priori* information. Further investigations using buoy data and data from field experiments in severe sea state, e.g., during the expedition ANT-XXV of R/V "Polarstern" (http://www.awi.de/en/infrastructure/ships/polarstern/weekly_reports/all_expeditions/), are in preparation.

Appendix A
List of Buoys Used for CWAVE_ENV Algorithm Validation

Name, latitude, and longitude of buoys used for the CWAVE_ENV empirical algorithm validation are given in Table IV. The positions of the buoys are shown in Fig. 2.

Appendix B
Estimation of ASAR Image Spectrum Using Periodogram Method

Estimation of the ASAR image spectrum is performed by computing the image periodogram with a 2-D FFT algorithm. The idea behind it is to divide the entire set with N samples into many subsets with M samples, to compute the FFT of each subset, to square it to get the power spectral density, and to compute the average of the ensemble. This approach implemented on the ASAR image spectral estimation is described in Appendix B.

A 2-D ASAR image with sizes of B_x and B_y in the range and azimuth directions is divided into nb_x and nb_y subscenes, respectively. The relation is given by

$$nb_x = B_x/n_x \qquad nb_y = B_y/n_y \tag{B1}$$

where $n_x = 256$ and $n_y = 512$ are taken to be the subscene sizes used to divide the entire samples of B_x and B_y in the range and azimuth directions. The 2-D FFT is performed on every subscene, i.e., normalized subscene G [computed via (8)] with pixel size n_x and n_y

$$F_G = fft_{nx*ny}(G). \tag{B2}$$

The power density spectrum for every subscene is denoted by P_S

$$P_S = (F_G)^2. \tag{B3}$$

Summing the subscene power density spectrum and averaging to reduce the variance, the entire ASAR image spectrum P is given by

$$P = \frac{1}{nb_x * nb_y} \sum P_S. \tag{B4}$$

The Fourier transform theory states that the integral of the image in the frequency domain is equal to the image variance in the spatial domain. The Cartesian spectrum computed in (B4) needs to be normalized to ensure this case. The normalized ASAR image spectrum is denoted as $\overline{P}$

$$\overline{P} = P * \left(\sum P * dk_x * dk_y \right)^{-1}. \tag{B5}$$

In (B5), dk_x, dk_y is the wavenumber spacing in the ASAR image range and azimuth directions, given by

$$dk_x = 2\pi/(B_x * d_x) \qquad dk_y = 2\pi/(B_y * d_y) \tag{B6}$$

where d_x, d_y is the pixel spacing in meters of the ASAR image.

The ASAR spectral parameters to be used for the CWAVE_ENV model are then computed from the ASAR image spectrum $\overline{P}$ by projection onto the subspace spanned by the orthonormal functions, i.e., by computing the respective scalar products

$$S = \sum \overline{P}(k_x, k_y)\overline{h_i}(k_x, k_y) dk_x dk_y \tag{B7}$$

where $1 \le i \le n_\varphi n_k$ and $\overline{h_i}$ are the orthonormal functions, and their exact forms are given in Appendix C.

Appendix C
Construction of Orthonormal Functions

The orthonormal functions $\overline{h_{ij}}$ used in the CWAVE_ENV model to extract ASAR image spectral parameters in

TABLE IV
NAME, LATITUDE, AND LONGITUDE OF BUOYS USED FOR VALIDATION, CORRESPONDING TO THE RED CROSS MARKS SHOWN IN FIG. 2

Station	Latitude	Longitude	Station	Latitude	Longitude
NODC_41001	34°44'N	72°41'W	**NODC_51001**	23°26'N	162°13'W
NODC_41002	32°19'N	75°22'W	**NODC_51002**	17°11'N	157°47'W
NODC_41009	28°30'N	80°10'W	**NODC_51003**	19°13'N	160°49'W
NODC_41010	28°57'N	78°29'W	**NODC_51004**	17°31'N	152°29'W
NODC_42001	25°54'N	89°40'W	**NODC_51028**	0°01'S	153°52'W
NODC_42002	25°10'N	94°25'W	**NODC_fpsn7**	33°29'N	77°35'W
NODC_42003	26°04'N	85°56'W	**NODC_46063**	34°16'N	120°42'W
NODC_42019	27°55'N	95°22'W	**NODC_46066**	52°42'N	154°59'W
NODC_42020	26°56'N	96°42'W	**NODC_46084**	56°35'N	136°10'W
NODC_42035	29°14'N	94°25'W	**MEDS_C44137**	42°17'N	62°00'W
NODC_42036	28°30'N	84°31'W	**MEDS_C44140**	43°45'N	51°45'W
NODC_42039	28°47'N	86°01'W	**MEDS_C44141**	43°00'N	58°00'W
NODC_42040	29°11'N	88°13'W	**MEDS_C44251**	46°26'N	53°23'W
NODC_44004	38°29'N	70°26'W	**MEDS_C44255**	47°17'N	57°21'W
NODC_44008	40°30'N	69°26'W	**MEDS_C44258**	44°30'N	63°24'W
NODC_44011	41°07'N	66°35'W	**MEDS_C46004**	50°56'N	136°05'W
NODC_44014	36°37'N	74°50'W	**MEDS_C46036**	48°21'N	133°56'W
NODC_44025	40°15'N	73°10'W	**MEDS_C46131**	49°55'N	124°59'W
NODC_46002	42°36'N	130°16'W	**MEDS_C46132**	49°44'N	127°56'W
NODC_46005	46°01'N	130°58'W	**MEDS_C46134**	48°40'N	123°29'W
NODC_46011	34°53'N	120°52'W	**MEDS_C46145**	54°22'N	132°25'W
NODC_46012	37°22'N	122°53'W	**MEDS_C46146**	49°20'N	123°44'W
NODC_46013	38°14'N	123°19'W	**MEDS_C46183**	53°37'N	131°06'W
NODC_46014	39°12'N	123°58'W	**MEDS_C46184**	53°55'N	138°51'W
NODC_46015	42°45'N	124°51'W	**MEDS_C46185**	52°25'N	129°49'W
NODC_46022	40°47'N	124°32'W	**MEDS_C46204**	51°22'N	128°45'W
NODC_46023	34°42'N	120°58'W	**MEDS_C46205**	54°10'N	134°17'W
NODC_46025	33°45'N	119°05'W	**MEDS_C46206**	48°50'	126°00'W
NODC_46027	41°51'N	124°23'W	**MEDS_C46207**	50°53'N	129°55'W
NODC_46028	35°44'N	121°53'W	**MEDS_C46208**	52°31'N	132°41'W
NODC_46029	46°08'N	124°31'W	**EUROP_41100**	15°54'N	57°54'W
NODC_46035	57°03'N	177°35'W	**EUROP_41101**	14°36'N	56°12'W
NODC_46042	36°45'N	122°25'W	**EUROP_62001**	45°12'N	5°00'W
NODC_46047	32°26'N	119°32'W	**EUROP_62029**	48°42'N	12°30'W
NODC_46050	44°38'N	124°30'W	**EUROP_62081**	51°00'N	13°24'W
NODC_46053	34°14'N	119°52'W	**EUROP_62105**	55°24'N	12°24'W
NODC_46059	38°02'N	130°00'W	**EUROP_62108**	53°30'N	19°24'W
NODC_46061	60°14'N	146°50'W	**EUROP_62163**	47°30'N	8°24'W
			EUROP_64045	59°06'N	11°42'W

wavenumber and angular dimensions are composed of Gegenbauer polynomials $g_i(\alpha_k)$ and harmonic functions $f_j(\alpha_\varphi)$, respectively

$$\overline{h_{ij}}(\alpha_k,\alpha_\varphi)=\eta(k_x,k_y)g_i(\alpha_k)f_j(\alpha_\varphi),\qquad 1\le i\le n_k;\quad 1\le j\le n_\varphi. \tag{C1}$$

In the CWAVE_ENV model, four Gegenbauer polynomials $g_i(\alpha_k)$ and five harmonic functions $f_j(\alpha_\varphi)$ are used, respectively, to generate the orthonormal functions

$$\begin{aligned}
g_1(\alpha_k)&=\frac{1}{2}\sqrt{3}\sqrt{1-\alpha_k^2}\\
g_2(\alpha_k)&=\frac{1}{2}\sqrt{15}\alpha_k\sqrt{1-\alpha_k^2}\\
g_3(\alpha_k)&=\frac{1}{4}\sqrt{\frac{7}{6}}\left(15\alpha_k^2-3\right)\sqrt{1-\alpha_k^2}\\
g_4(\alpha_k)&=\frac{1}{4}\sqrt{\frac{9}{10}}\left(35\alpha_k^3-15\alpha_k^2\right)\sqrt{1-\alpha_k^2}
\end{aligned}\tag{C2}$$

$$\begin{aligned}
f_1(\alpha_\varphi)&=\sqrt{1/\pi}\\
f_2(\alpha_\varphi)&=\sqrt{2/\pi}\ \sin(2\alpha_\varphi)\\
f_3(\alpha_\varphi)&=\sqrt{2/\pi}\ \cos(2\alpha_\varphi)\\
f_4(\alpha_\varphi)&=\sqrt{2/\pi}\ \sin(4\alpha_\varphi)\\
f_5(\alpha_\varphi)&=\sqrt{2/\pi}\ \cos(4\alpha_\varphi).
\end{aligned}\tag{C3}$$

In (C2) and (C3), α_k and α_φ are the definitions of integration area A in the wavenumber domain of the ASAR image spectra. Considering the velocity bunching effect of SAR imaging surface waves, which leads to a bunching wave spectrum in the SAR azimuth direction, the integration area A is chosen as an elliptic shape. α_k and α_φ are defined respectively as

$$\alpha_k(k_x,k_y)=2\frac{\log\sqrt{a_1k_x^4+a_2k_x^2+k_y^2}-\log\ k_{\min}}{\log\ k_{\max}-\log\ k_{\min}}-1 \tag{C4}$$

$$\alpha_\varphi(k_x,k_y)=\arctan(k_y,k_x). \tag{C5}$$

$$\eta(k_x,k_y)=\left(\frac{2\left(a_2k_x^2+2a_1k_x^4+k_y^2\right)}{\left(k_x^2+k_y^2\right)\left(a_2k_x^2+a_1k_x^4+k_y^2\right)\left(\log\ k_{\max}-\log\ k_{\min x}\right)}\right)^{\frac{1}{2}} \tag{C9}$$

The maximum wavenumber $k_{\max}$ used in the integration area A is

$$k_{\max}=2\pi/(60\text{ m}) \tag{C6}$$

where corresponding to the shortest wavelength of surface waves is 60 m, which is on the order of twice the sensor spatial resolution. The minimum wavenumber $k_{\min}$ is set to

$$k_{\min}=2\pi/(624\text{ m}). \tag{C7}$$

Wavenumbers less than $k_{\min}$, which generally are associated with atmospheric features observed in SAR imagery, are excluded from the integration area A.

Two parameters a_1 and a_2 in (C4) are defined as

$$a_1=\frac{\gamma^2-\gamma^4}{\gamma^2k_{\min}^2-k_{\max}^2}$$
$$a_2=\frac{k_{\max}^2-\gamma^4k_{\min}^2}{k_{\max}^2-\gamma^2k_{\min}^2} \tag{C8}$$

where $\gamma=2$ is the parameter describing the bunching effect in the SAR imaging process, i.e., the ratio of the highest wavenumber in the respective range and azimuth in domain A.

In (C1), $\eta(k_x,k_y)$ is the weight function defined in (C9), shown at the top of the page. Substituting (C2), (C3), and (C9) into (C1), one can obtain the orthonormal functions to extract ASAR image spectral parameters used in the CWAVE_ENV model.

ACKNOWLEDGMENT

The authors would like to thank ESA for providing the ASAR data and the collocated ECMWF reanalysis WAM and buoy measurements, the TU Delft Radar Altimeter Database System and CERSAT system for the RA, and Dr. J. Schulz-Stellenfleth from GKSS and Prof. H. Grassl from the University of Hamburg for the discussions and comments.

REFERENCES

[1] R. C. Beal, D. G. Tilley, and F. M. Monaldo, "Large- and small-scale spatial evolution of digitally processed ocean surface wave spectra from the SEASAT synthetic aperture radar," *J. Geophys. Res.*, vol. 88, no. C3, pp. 1761–1778, 1983.

[2] P. G. Challenor and P. D. Cotton, "The joint calibration of altimeter and *in situ* wave heights," in *Advances in the Applications of Marine Climatology|The Dynamic Part of the WMO Guide to the Applications of Marine Climatology*, JCOMM Tech. Rep. 13, WMO/TD-No. 1081, 2003, World Meterol. Org., Geneva, Switzerland.

[3] P. Queffeulou, "Long-term validation of wave height measurements from altimeters," *Mar. Geod.*, vol. 27, no. 3, pp. 495–510, Jul. 2004.

[4] C. P. Gommenginger, M. A. Srokosz, P. G. Challenor, and P. D. Cotton, "Measuring ocean wave period with satellite altimeters: A simple empirical model," *Geophys. Res. Lett.*, vol. 30, no. 22, p. 2150, Nov. 2003. DOI: 10.1029/2003GL017743.

[5] Y. Quilfen, B. Chapron, F. Collard, and M. Serre, "Calibration/validation of an altimeter wave period model and application of TOPEX/Poseidon and JASON-1 altimeters," *Mar. Geod.—Special Issue on Jason1 Calibration/Validation III*, vol. 27, no. 3/4, pp. 535–549, Jul. 2004.

[6] E. B. L. Mackay, C. H. Retzler, P. G. Challenor, and C. P. Gommenginger, "A parametric model for ocean wave period from K_u band altimeter data," *J. Geophys. Res.*, vol. 113, no. C3, p. C03 029, Mar. 2008. DOI: 10.1029/2007JC004438.

[7] K. Hasselmann, R. K. Raney, W. J. Plant, W. Alpers, R. A. Shuchman, D. R. Lyzenga, C. L. Rufenach, and M. J. Tucker, "Theory of synthetic aperture radar ocean imaging: A MARSEN view," *J. Geophys. Res.*, vol. 90, no. C7, pp. 4659–4686, 1985.

[8] W. Alpers and C. Brüning, "On the relative importance of motion-related contributions to the SAR imaging mechanism of ocean surface waves," *IEEE Trans. Geosci. Remote Sens.*, vol. GRS-24, no. 6, pp. 873–885, Nov. 1986.

[9] G. Engen and H. Johnson, "SAR-ocean wave inversion using image cross spectra," *IEEE Trans. Geosci. Remote Sens.*, vol. 33, no. 4, pp. 329–360, Jul. 2000.

[10] K. Hasselmann and S. Hasselmann, "On the nonlinear mapping of an ocean wave spectrum into a synthetic aperture radar image spectrum," *J. Geophys. Res.*, vol. 96, no. C6, pp. 10 713–10 729, 1991.

[11] H. E. Krogstad, "A simple derivation of Hasselmann's nonlinear ocean-synthetic aperture radar transforms," *J. Geophys. Res.*, vol. 97, no. C2, pp. 2421–2425, Feb. 1992.

[12] P. Heimbach, S. Hasselmann, and K. Hasselmann, "Statistical analysis and intercomparison with WAM model data of three years of global ERS-1 SAR wave mode spectral retrievals," *J. Geophys. Res.*, vol. 103, no. C4, pp. 7931–7977, 1998.

[13] G. Brooker, "UWA processing algorithm specification," ESA, Noordwijk, The Netherland, 1995.

[14] C. Mastenbroek and C. de Valk, "A semi-parametric algorithm to retrieve ocean wave spectra from synthetic aperture radar," *J. Geophys. Res.*, vol. 105, no. C2, pp. 3497–3516, 1998.

[15] J. Schulz-Stellenfleth, S. Lehner, and D. Hoja, "A parametric scheme for the retrieval of two-dimensional ocean wave spectra from synthetic aperture radar look cross spectra," *J. Geophys. Res.*, vol. 110, p. C05 004, May 2005. DOI: 10.1029/2004JC002822.

[16] S. Lehner, J. Schulz-Stellenfleth, J. B. Schättler, H. Breit, and J. Horstmann, "Wind and wave measurements using complex ERS-2 wave mode data," *IEEE Trans. Geosci. Remote Sens.*, vol. 38, no. 5, pp. 2246–2257, Sep. 2000.

[17] *Envisat ASAR Product Handbook*, Eur. Space Agency, Noordwijk, The Netherlands, Issue 2.2, 2007.

[18] X.-M. Li, T. König, J. Schulz-Stellenfleth, and S. Lehner, "Validation and intercomparison of ocean wave spectra retrieval scheme using ASAR wave mode data," *Int. J. Remote Sens.*, 2010, to be published.

[19] J. Schulz-Stellenfleth, T. König, and S. Lehner, "An empirical approach for the retrieval of integral ocean wave parameters from synthetic aperture radar data," *J. Geophys. Res.*, vol. 112, no. C3, p. C03 019, Mar. 2007. DOI: 10.1029/2006JC003970.

[20] J. Schulz-Stellenfleth and S. Lehner, "Measurement of 2-D sea surface elevation fields using complex synthetic aperture radar data," *IEEE Trans. Geosci. Remote Sens.*, vol. 42, no. 6, pp. 1149–1160, Jun. 2004.

[21] WAMDI GROUP, "The WAM model—A third generation ocean wave prediction model," *J. Phys. Oceanogr.*, vol. 18, pp. 1775–1810, 1984.

[22] H. Günther, S. Hasselmann, and P. A. E. M. Janssen, "The WAModel cycle 4 (revised version)," Deutsches Klimarechenzentrum (DKRZ), Hamburg, Germany, 1992.

[23] P. A. E. M. Janssen, "Progress in ocean wave forecasting," *J. Comput. Phys.*, vol. 227, no. 7, pp. 3572–3594, Mar. 2008.

[24] A. Behrens and H. Günther, "Operational wave prediction of extreme storms in Northern Europe," *Nat. Hazards*, vol. 49, no. 2, pp. 387–399, May 2008.

[25] S. Caires and A. Sterl, "Validation of ocean wind and wave data using triple collocation," *J. Geophys. Res.*, vol. 108, no. C3, p. 3098, Mar. 2003. DOI: 10.1029/2002JC001491.

[26] J. G. Li, P. Wittmann, M. Fauchon, H. Chen, J. M. Lefevre, T. Bruns, D. Greenslade, F. Ardhuin, N. Kohno, S. Park, and M. Gomez, "Intercomparison of operational wave forecasting systems," in *Proc. 10th Int.*

Workshop Wave Hindcasting Forecast. Coastal Hazard Symp., Oahu, HI, Nov. 11–16, 2007.
[27] K. E. Steele and M. D. Earle, "The status of data produced by NDBC wave data analyzer (WDA) system," in *Proc. Oceans*, San Diego, CA, 1979, pp. 212–220.
[28] H. von Storch and F. Zwiers, *Statistical Analysis in Climate Research*. NewYork: Cambridge Univ. Press, 1999.
[29] V. Kerbaol, B. Chapron, and P. W. Vachon, "Analysis of ERS-1/2 synthetic aperture radar wave mode imagettes," *J. Geophys. Res.*, vol. 103, no. C4, pp. 7833–7846, 1998.
[30] A. Stoffelen and D. Anderson, "Scatterometer data interpretation: Estimation and validation of the transfer function CMOD4," *J. Geophys. Res.*, vol. 102, no. C3, pp. 5767–5780, 1997.
[31] S. Lehner, J. Horstmann, and W. Koch, "Mesoscale wind measurements using recalibrated ERS SAR images," *J. Geophys. Res.*, vol. 103, no. C4, pp. 7847–7856, 1998.
[32] V. Swail, "Requirements for wave observations," World Meteorol. Org., Geneva, Switzerland, Doc. WMO/TD-1466, JCOMM Tech. Rep. 47, 2008.
[33] X.-M. Li, S. Lehner, and W. Rosenthal, "Investigation of ocean surface wave refraction using TerraSAR-X data," *IEEE Trans. Geosci. Remote Sens.*, vol. 48, no. 2, pp. 830–840, Feb. 2010.
[34] P. D. Cotton, P. G. Challenor, and D. J. T. Carter, "An assessment of the accuracy and reliability of GEOSAT, ERS-1, ERS-2 and TOPEX altimeter measurements of significant wave height and wind speed," in *Proc. CEOS Wind Wave Valid Workshop*, 1997, pp. 81–93.
[35] H. E. Krogstad and S. F. Barstow, "Satellite wave measurements for coastal engineering applications," *Coast. Eng.*, vol. 37, no. 3, pp. 283–307, Aug. 1999.
[36] *Guide to Wave Analysis and Forecasting*, World Meteorol. Org. (WMO), 2nd ed., Geneva, Switzerland, 1998.
[37] S. K. Gulev, V. Grigorieva, A. Sterl, and D. Woolf, "Assessment of the reliability of wave observations from voluntary observing ships: Insights from the validation of a global wind wave climatology based on voluntary observing ship data," *J. Geophys. Res.*, vol. 108, no. C7, p. 3236, 2003. DOI: 10.1029/2002JC001437.
[38] WASA, "Changing waves and storms in the Northeast Atlantic?" *Bull. Amer. Meteorol. Soc.*, vol. 79, no. 5, pp. 741–760, May 1998.
[39] X. L. Wang and V. R. Swail, "Changes of extreme wave heights in Northern Hemisphere oceans and related atmospheric circulation regimes," *J. Clim.*, vol. 14, no. 10, pp. 2204–2221, May 2001.
[40] A. Sterl and S. Caires, "Climatology, variability and extrema of ocean waves: The web-based KNMI/ERA-40 wave atlas," *Int. J. Climatol.*, vol. 25, no. 7, pp. 963–997, Jun. 2005.
[41] D. K. Woolf, P. G. Challenor, and P. D. Cotton, "Variability and predictability of the North Atlantic wave climate," *J. Geophys. Res.*, vol. 107, pp. 3145–3158, Oct. 2002.
[42] T. König, S. Lehner, and J. Schulz-Stellenfleth, "Global analysis of a 2 year ERS-2 wave mode dataset over the ocean," in *Proc. IGARSS*, Barcelona, Spain, 2007.
[43] J.-M. Lefèvre and L. Aouf, "Use of wind/wave satellite data for numerical wave predictions at Meteo-France," in *Proc. Globe Wave Workshop*, Brest, France, Sep. 19–21, 2007.
[44] G. Dietrich, K. Kalle, W. Krauss, and G. Siedler, "Allgemeine Meereskunde," in *Eine Einfruehrung in die Ozeanographie*. Berlin, Germany: Gebrueder Borntraeger, 1975.

Xiao-Ming Li received the B.S. degree in electronics and information engineering from Xi'an Communication College of the People's Liberation Army, Xi'an, China, in 2002, the (equivalent) M.S. degree, with work focusing on satellite ocean remote sensing, from the Ocean University of China, Qingdao, China, in 2006, and the Ph.D. degree in geophysics from the University of Hamburg, Hamburg, Germany, in 2010.

Since 2006, he has been with the Remote Sensing Technology Institute, German Aerospace Center (DLR), Wessling, Germany. His research interests include synthetic aperture radar ocean wave algorithm development, investigation of extremely oceanic weather, and observation of ocean dynamics using spaceborne multisensors.

Susanne Lehner received the M.Sc. degree in applied mathematics from Brunel University, Uxbridge, U.K., in 1979 and the Ph.D. degree in geophysics from the University of Hamburg, Hamburg, Germany, in 1984.

She was a Research Scientist with the Max Planck Institute for Meteorology, Hamburg. In 1996, she joined the German Remote Sensing Data Center, German Aerospace Center (DLR), Wessling, Germany, where she is currently a Research Scientist in marine remote sensing with the Remote Sensing Technology Institute, working on the development of algorithms determining marine parameters from synthetic aperture radar.

Thomas Bruns received the Diploma degree in meteorology from the University of Hamburg, Hamburg, Germany, in 1981 and the Ph.D. degree from the Max Planck Institute for Meteorology, Hamburg, in 1985.

Since 1987, he has been with the German Weather Service (DWD), Hamburg, specializing in marine and arctic meteorology, ocean wave modeling, ship routing, marine weather forecast, and aviation weather forecast.

Dr. Bruns has been a member of the Expert Team on Wind Waves and Storm Surges, Joint WMO–IOC Technical Commission for Oceanography and Marine Meteorology since 2007.